NO 2

FILE NO.

FILE COPY NO. 2

TECHNICAL MEMORANDUMS

NATIONAL ADVISORY COMMITTEE FOR AERONAUTICS

No. 830

METHOD OF CURVED MODELS AND ITS APPLICATION TO THE STUDY OF CURVILINEAR FLIGHT OF AIRSHIPS

P A R T II

By G. A. Gourjienko

Central Aero-Hydrodynamical Institute, Moscow, 1934

THIS DOCUMENT ON LOAN FROM THE FILES OF

NATIONAL ADVISORY COMMITTEE FOR AERONAUTICS
LANGLEY MEMORIAL AERONAUTICAL LABORATORY
LANGLEY FIELD, HAMPTON, VIRGINIA

RETURN TO THE ABOVE ADDRESS.

REQUESTS FOR PUBLICATIONS SHOULD BE ADDRESSED AS FOLLOWS:

NATIONAL ADVISORY COMMITTEE FOR AERONAUTICS
1724 F STREET, N.W.,
WASHINGTON 25, D.C.

Washington
June 1937

NATIONAL ADVISORY COMMITTEE FOR AERONAUTICS

TECHNICAL MEMORANDUM NO. 830

METHOD OF CURVED MODELS AND ITS APPLICATION TO THE STUDY OF CURVILINEAR FLIGHT OF AIRSHIPS*

By G. A. Gourjienko

P A R T II

For carrying out the first experiments according to the method of curved models, we found it most convenient to construct and test a model of the nonrigid V-2 airship "Smolny" (capacity 5,000 cubic meters). The selection of this airship was motivated, in the first place, by the fact that we had at our disposal a large amount of material relating to aerodynamic tests of the noncurved model (to the scale of 1/64.64 of the full-scale size), including also detailed tests on rotary derivatives, carried out by the aid of the method of damped oscillations and, in the second place, by the fact that at the present time we have the results of flight tests of this airship, which were made for the purpose of determining the radius of turn. In this manner, we are able to compare the results, obtained by the aid of the method of curved models, with the results of tests made by the aid of the method of damped oscillations, and with flight tests. Consequently, we shall be able to judge which method of testing in the tunnel produces results that are in closer agreement with flight test results.

At the outset we proposed that the method of curved models be used only as a verifying method, since, according to the above, in order to use this method as an independent method, it is necessary to construct a very large number of models of various degrees of curvature. However, we have found lately that we can use our model with a very high degree of accuracy, for carrying out that number of experiments which will make it possible to use the method of curved models as an independent method, that is to say, which will give the relations of the rotary derivatives

*Report No. 182, of the Central Aero-Hydrodynamical Institute, Moscow, 1934.

of the forces and the moment in terms of β_o or in terms of δ and in the final result, the nomogram

$$\frac{1}{R_o} = f(\beta_o, \delta)$$

Thus, the ultimate object of this work is to construct this nomogram, compare it with the results of previous tests and with flight test results.

We shall show below the considerations on the basis of which it may be permissible to use one model for obtaining an exhaustive number of results.

1. MODEL

For constructing the curved axis we have taken the values of R_o and β_o, which are obtained from the nomogram $\frac{1}{R} = f(\beta_o, \delta)$ by turning the dirigible with the minimum radius (fig. 16).

When $\delta = 30^o$, these values are:

$$R_o = 2.325 \text{ m}$$

$$\beta_o = 8^o\ 51'$$

Thus, the equation of the curved axis according to formula (7) will be:

$$z' = 2.3\left(\text{ch}\frac{x}{2.3} - 1\right)$$

In accordance with the simplified method of construction described above, the cross sections were assumed plane.

For the distance of the origin of the coordinates (point B) from the nose of the model, according to formula (30), we obtained:

$$x_{1_B} = 0.0505 \text{ m}$$

The relation of the abscissa x to the length of the curved axis is obtained from formula (8):

$$x = 2.3 \text{ Ar sh } \frac{x_1}{2.3}$$

Figure 17 represents a diagram of the curved V-2 model, constructed by the aid of the formulas indicated.

The coordinates x and z' of the curved axis, as well as the length of the arc of the axis x_1 and the ordinates y_1 of the contour, laid off on the normals away from the axis, are given in Table I as a function of the reading along the arc of the curved axis (X_1), read off from the nose of the model.

The tail surfaces of the model were deformed according to the rule indicated on page 26 of Part I (Technical Memorandum No. 829). The gondola of the airship remained uncurved since curving it would have involved unnecessary additional difficulties. But the effect of the curvature of the gondola (due to the fact that it is located at a very short distance away from the center of displacement) on the results of the experiment must be very small and must be definitely within the limits of experimental error. The gondola was installed on the model along the tangent to the curved axis at the point of installation.

The hull of the model, the gondola, and the tail surfaces were constructed at the workshops of the Experimental Aerodynamic Department of the Central Aero-Hydrodynamic Institute. The hull was hollow in the interior (with a wall thickness of 15 mm), and was turned of beech.

2. POSSIBILITY OF USING ONE CURVED MODEL FOR CONDUCTING AN EXHAUSTIVE NUMBER OF EXPERIMENTS

It was shown above that, for an exhaustive use of the method, it is necessary, for a given series of values of R_0 and β_0, to construct as many models as there are possible combinations of R_0 and β_0.

To begin with, let us leave out of consideration the angle β_0 and let us assume that we have prepared a series of models with β_0 = const. and R_0 = variable.

In testing such a series in the tunnel, by changing R_0, we change the angular velocity of turning along the circle $\left(\omega_y = \frac{v_0}{R_0}\right)$

But, according to the series of investigations abroad, the rotary derivative of the moment does not depend on the angular velocity, that is to say, the terms of the higher orders (beginning with the second order) of the series (formula (34)) becomes zero*.

The rotary derivatives of the forces to some extent depend on the angular velocity.

However, these derivatives too may be considered with a sufficiently large degree of accuracy as independent of ω_y.

Admitting the assumption that the rotary derivatives are independent of the angular velocity, we ought to admit, as a consequence, that these derivatives, determined by the formulas (38) for the entire series indicated (when β_0 = constant), should be individually equal.

But, we have no right to change the angular velocity by reason of the change in v_0 $\left(\omega_y = \frac{v_0}{R_0}\right)$, since the rotary derivatives and the aerodynamic factors of the formulas (38) (on the right sides) assume a form that is not dependent on the linear velocity v_0**.

Thus, by testing one model at the given angle β_0, we obtain the values of the rotary derivatives during flight with various radii, but with β_0 = constant.

Now, let us examine the series of models, constructed

*This is confirmed by the fact that, during all the tests on rotary derivatives of the moment, the logarithmic damping decrement and the oscillation period do not depend on time and, consequently, do not depend on angular velocity.

**Besides, a variation in the linear velocity does not change the distribution of the local angles of attack along the model axis, i.e., it does not change the physical phenomenon.

with R_o = const. and β_o = var. Let us turn to figure 18. Here the curve A - A represents the curved axis of our model in the position in which the tangent to it, drawn at the center of volume, forms with the axis of the tunnel the angle $\beta_o = 8^o 51'$. Let us assume that, by placing our model on the pole of the moment instrument (passing through the center of volume), we turn it about the axis y until our tangent coincides with the tunnel axis, that is to say, β_o becomes zero. This position of the curved axis is expressed in the form of the curve B - B. The curve C - C with several points, indicated by circles, represents the axis of that curved model of the series R_o = const., β_o = var., which is constructed with R_o = 2.325 m and β_o = 0.

As will be seen, this axis differs very little from the B - B curve. Only at the stern is there a small divergence; the nose parts of the axis merge. It is obvious that all the other axes of the series of models R_o = const. = 2.325 m and β_o = var. should differ still less from the axis of our model, since $\beta_o = 0$ and $\beta_o = 8^o 51'$ embrace the entire range of angles of attack with which we are concerned.

All this naturally suggests that our one curved model can be tested with complete satisfaction at the angles of attack, like any straight model, obtaining in addition the relations of the rotary derivatives to the angles of attack. Below, in the division "Working up of the test data and corrections thereto," we shall show how we have made the attempt to introduce a correction to the experimental results for this difference in the curvature of the stern.

3. METHOD OF PRODUCING A VELOCITY GRADIENT ACROSS THE TUNNEL

The problem of creating a velocity gradient across the tunnel can be solved by installing in front of the model in the tunnel a special device which distributes the flow in accordance with the requisite rule. In our opinion, such a device may be either a nozzle, divided into cells, the area of the sections of which varies along the diameter of the tunnel, or it may be a netting of variable mesh.

For working out the problem we have taken the latter device (the variable mesh netting). In our opinion, it

has more advantages as compared to the first device, since the netting is easier to prepare, gives a smoother distribution of velocity and offers less obstruction in the kinetic section of the tunnel.

The first netting was constructed in accordance with the following considerations.

Let us turn to figure 19. The upper half of the diagram represents a section of the working section of the tunnel, in which a netting of constant mesh T is installed (T is the number of threads per meter in the net). Then, considering the velocity in the tunnel as constant and equal to v_0, we may write that the reduction in the pressures $P_{1_0} - P_{2_0}$ resulting from the netting resistance is equal to the losses due to the netting resistance:

$$P_{1_0} - P_{2_0} = \frac{C_x \rho S v_0^2 n}{a\, l} \tag{39}$$

Here C_x is the coefficient of drag of one wire of the netting, ρ is the density of the air, n is the number of all the wires, S and a are the midship section and the length of one wire, l is the width of the netting.

It is obvious that $\frac{S}{a} = d_n$ (diameter of the wire), and $\frac{n}{l} = T$. Then formula (39) is transformed as follows:

$$P_{1_0} - P_{2_0} = C_x \rho\, d_n\, v_0^2\, T \tag{40}$$

Considering that all the wires are of equal length a, we find that the resistance of the part of the netting bounded by the sections, which are at a distance of $\pm z$ from the tunnel axis, is equal to:

$$F_0 = \int_{-z}^{z} (P_{1_0} - P_{2_0})\, a\, dz = a \int_{-z}^{z} C_x \rho\, d_n\, v_0^2\, T\, dz$$

Here z is the variable ordinate, read off crosswise to the right and to the left of the tunnel axis.

Since T = const., we obtain from the preceding equation:

$$F_o = 2\, C_x\, \rho\, a\, d_n\, v_o^2\, T\, z \qquad (41)$$

Now, let us look at the lower half of figure 18, where we have transposed our wires along the ordinate z in such a way that we obtained a netting with variable mesh t. The number of all the wires n remained unchanged, and their distance apart on the tunnel axis remained equal to T.

Then, analogously to formula (40) for the section, which is at a distance z from the axis, we find that the local reduction in pressure $P_1 - P_2$ will be:

$$P_1 - P_2 = C_x\, \rho\, d_n\, v^2\, t$$

Here v is the local velocity in section z (since $t > T$, then $v < v_o$). The total resistance of the part of the variable mesh netting, similar to the part described above, will be:*

$$F = \int_{-z}^{z} (P_1 - P_2)\, a\, dz = a\, C_x\, \rho\, d_n \int_{-z}^{z} v^2\, t\, dz \qquad (42)$$

Here v and t are variables and are functions of z.

Since the number of wires in case I and case II (fig. 18) remain unchanged, it is evident that the resistance of the part of the netting with constant mesh, which we have examined, will be equal to the resistance of the part of the variable mesh netting, that is to say,

$$F_o = F$$

and

$$2\, C_x\, \rho\, a\, d_n\, v_o^2\, Tz = C_x\, \rho\, a\, d_n \int_{-z}^{z} v^2\, t\, dz$$

that is to say,

$$2\, v_o^2\, Tz = \int_{-z}^{z} v^2\, t\, dz$$

Differentiating both sides of the equation obtained, we find:

$$v_o^2\, T = v^2 t$$

*The mutual influence of the elements of the netting are not taken into account here, thereby involving a certain error, which will be corrected later on.

hence we find that

$$\frac{v_0^2}{v^2} = \frac{t}{T} \tag{43}$$

that is to say, the squares of the velocities, obtained as a result of installing the netting with variable mesh, are inversely proportional to the local distances apart of the wires of the netting.

Thus, any distribution of velocity can be easily obtained behind the netting, by constructing it in accordance with the law, obtained from formula (43):

$$t = T\left(\frac{v_0}{v}\right)^2 \tag{44}$$

The necessary linear law of velocity distribution, expressed according to formula (33) as

$$\frac{v}{v_0} = 1 + \frac{z}{R_0}$$

can be obtained, consequently, by constructing the netting in accordance with the law

$$t = \frac{T}{\left(1 + \frac{z}{R_0}\right)^2} \tag{45}$$

obtained by substituting $\frac{v}{v_0} = 1 + \frac{z}{R_0}$ in formula (44).

Such a netting was constructed by us from two-millimeter paraffined cord. The distance between the wires of the netting along the tunnel axis was selected $T = 150 \frac{\text{threads}}{1 \text{ m}}$, which corresponds to the distance between the cords $\frac{1}{T} = 6.67$ mm. It is clear that the netting was variable only across the tunnel along the horizontal. But

along the vertical, for each 100 millimeters, the individual cords of the netting were intertwined with thin threads. These threads extinguised the cord vibrations that might have occurred in the flow.

The netting was stretched on a wooden frame 800 by 800 millimeters, which was suspended in the tunnel. The frame was provided at the sides with streamlined fairings made of stiff lacquered paper.

Since it is extremely difficult to use the formula (45) directly, in stretching the netting we made use of the relation between the distance of any cord from the tunnel axis and the mesh which is supposed to be on this distance. This relation may be obtained in the following manner.

Let us find a certain curve $x = f(z)$ (fig. 20), which has the characteristic that the constant increment of the function Δx gives the variable increment of the argument z, equal to AB, that is to say, to the distance between two adjacent cords of the netting, the first of which is coordinated with the magnitude z.

It is clear that the distance $AB = \frac{1}{t}$. From figure 20 we see that

$$\frac{\Delta x}{\frac{1}{t}} = \tan a = \frac{dx}{dz}$$

whence

$$x = \int \Delta x t \, dz$$

substituting, in the obtained integral t according to formula (45), we find that

$$x = \int \frac{\Delta x T dz}{\left(1 + \frac{z}{R}\right)^2} + C$$

Integrating and discarding C as a quantity which has an influence only on the altitudinal position of the curve $x = f(z)$ and, consequently, does not change the characteristic of the curve, with which we are concerned, we find that

$$x = - \frac{T R_0 \Delta x}{1 + \frac{z}{R_0}}$$

This will give us the desired distance of any cord from the tunnel axis:

$$z = - R_0 \left(1 + \frac{\Delta x T R_0}{x} \right) \qquad (46)$$

In this formula it is necessary to consider x as changing in progression, that is to say,

$$x = x_1 + \Delta x; \quad x = x_1 + 2 \Delta x; \quad x = x_1 + 3 \Delta x \quad \text{etc.}$$

where x_1 = constant. The magnitude Δx can be found at one's discretion.

The netting, constructed by the aid of the methods described above, was stretched in the working section of the tunnel T-3 (D = 1,5 m) by the aid of twelve wires with tenders. (The netting and its installation are clearly shown in figs. 24 and 25). Then, behind the netting, at a velocity of from 34 to 35 meters per second, the field of velocities was carefully explored by the aid of Prandtl's tube. The field was explored in two sections (150 mm and 800 mm from the netting) along the horizontal lines parallel to the netting and lying in the plane passing through the tunnel axis.

In the first section readings were taken for every 20 millimeters of the coordinate z, in the second section readings were taken for every 10 millimeters.

The test was made by the aid of two micromanometers according to the method of instantaneous readings; one of the micromanometers was connected to the movable Prandtl tube and the other was connected to the tunnel speed control device. Such a plan of testing allowed us, when exploring the field, to take into account the pulsation of the flow according to the velocity, since, before exploring the field, the movable speed device was adjusted to the speeds in accordance with the readings

on the speed control device. During this adjustment the movable speed indicator was on the tunnel axis ($z = 0$). In this manner, knowing during each instantaneous reading (making use of the adjustment indicated) the velocity along the tunnel axis, it was possible to find the relation of the velocity at any point along the straight line investigated to the velocity along the tunnel axis.

This relation was calculated according to the obvious correlation

$$\frac{v}{v_0} = \sqrt{\frac{h}{h_0}}$$

where h is the reading on the movable speed indicator, and h_0 is the reading on the speed indicator on the tunnel axis, determined according to the adjustment indicated above.

In figure 21 there are plotted the results of these tests as a function of z. The values $\frac{v}{v_0}$ in the first section are indicated by crosses; the values $\frac{v}{v_0}$ in the second section are indicated by points.

Besides, on the same graph there are plotted: (1) the necessary distribution of velocity, according to formula (33) when $R_0 = 2.325$ m (designated by $\left[\frac{v}{v_0}\right]_{theor.}$); (2) the distance apart of the wires of the netting $t = f(z)$, obtained according to formula (45) (designated by $t_{theor.}$).

As will be seen, nearly all the experimental points lay below the straight line $\left[\frac{v}{v_0}\right]_{theor.}$. Thus, judging from the first tests, the netting did not come up to expectation. This was due to the fact that, in constructing the netting, we disregarded the mutual influence of the cords, for which reason the support (loss of velocity) came out everywhere greater than calculated.

Therefore, in order to create the necessary velocity

distribution, it was decided to correct the netting by "shifting" its mesh. A mean curve was drawn through the experimental points of section II (designated by $\left[\frac{v}{v_o}\right]_{experimental}$).*

The mesh was "shifted" in the following manner. The mesh, corresponding to point A of the curve $t_{theoretical} = f(z)$, produced a velocity relation $\left[\frac{v}{v_o}\right]_{experimental}$, determined by point B on the curve $\left[\frac{v}{v_o}\right]_{experimental} = f(z)$ when $z = 0.275$. Such a velocity relation is necessary to have (according to the straight line $\left[\frac{v}{v_o}\right]_{theor.}$ not for $z = 0.275$ but for $z = 0.175$ (point C). For this purpose we have to "shift" the mesh at point A parallel to the straight line BC by the magnitude $z = 0.275 - 0.175 = 0.1$ m. In this manner we obtain point E.

Proceeding thus with every point on the curve $t_{theoretical}$, a new arrangement of the netting mesh was obtained; it was designated by $t_{corrected}$. The netting was stretched again according to the new arrangement of the mesh and tested by the aid of methods that are entirely analogous to the method described above. As will be seen from figure 22, the velocity distribution both in section I as well as in section II coincides very well with the requisite rectilinear distribution, that is to say, the divergences in section II nowhere (within the limits of the necessary zone where the gradient is produced) exceed 2 to 3 percent.

Thus, the problem concerning the velocity gradient was solved by us satisfactorily in principle.

*The advantage of the second section over the first consists in the fact that in the region of the second section there are supposed to be installed the tail surfaces of the model; these tail surfaces are supposed to have the greatest influence on the magnitudes of the rotary derivatives.

4. EXPERIMENTS

The curved model was tested in the closed working part of the T-3 tunnel. The selection of this tunnel for carrying out the experiments was motivated by the following facts:

1. The section of this tunnel and its other dimensions closely correspond to the section and dimensions of the NK-1 tunnel, where we have previously conducted the experiments on the rotary derivatives. In this manner, the results may be compared with greater reliability.

2. The two-component scale of this tunnel, on which the model is installed by the aid of holders, allows us to work up the record sheets much more simply than in the case of other systems of securing the model.

3. The velocity in this tunnel may be very high, which permits us to attain, behind the netting, from 35 to 40 meters per second, in spite of the very great total resistance of the netting.

In order to ascertain the influence of the velocity gradient on the results of the curved model tests, the tests were carried out with and without the netting in position; the velocity along the tunnel axis behind the netting was taken equal to the velocity of the free flow.

In both cases, in order to obtain results with a maximum possible degree of reliability and to ascertain the relation of the rotary derivatives both to the angle of attack and to the rudder angle of deviation δ, a great many tests were made, that is to say, with every one of the selected rudder angles of deviation $\delta = 0; 5; 10; 15; 20; 25; 30; 35; 40; 45$ degrees, tests were made at the following angles of attack

$$\beta_o = 0; 2; 4; 5; 6; 7; 8; 9; 10; 11; 12; 13; 14 \text{ degrees.}$$

Such angles of rudder deviation δ, as 40 degrees and 45 degrees, which would seem to be too large, were taken for the purpose of ascertaining at what point the rudder stops being effective when the ship turns.

The angles β_o were taken only on one side, because, during circular flight, the ship's nose is never outside

the trajectory. The large distance apart of the angles β_o (1° apart) was selected due to our desire to investigate completely those peculiar bends in the curve.

$\left[\frac{1}{v_o}\frac{\partial M_y}{\partial \omega_y}\right] = f(\beta_o)$, which we found in the case of the old tests.

In accordance with the preceding notation, the angle formed by the tunnel axis and the tangent to the curved axis of the model at the center of volume was taken as the angle of attack β_o.

Figure 23 shows a diagram of the installation of the model in the tunnel (on the moment apparatus) and indicates the direction of the angles β_o and δ (which correspond to circular turning). The photographs (figs. 24 and 25) show this installation.

Besides testing the curved model with tail surfaces, there were also tested at the same angles β_o a bare curved hull and a hull with a gondola (which enabled us to find very interesting relations of the rotary derivatives of the bare hull to the angle of attack).

Simultaneously with the curved model, tests were carried out in an analogous manner (without the netting) with the straight V-2 model, which had never yet been tested in detail in the given tunnel.

The aerodynamic moment was measured on the conventional moment apparatus. The results of all the tests on the moment are given in the form of coefficients of R in figure 26. Here (for a comparison of the change in all coefficients according to the angles of attack β_o) all the curves are given to the same scale: $R_{\Sigma M}$ is the coefficient of the curved model moment, R_{m_y} is the coefficient of the straight model moment. As will be seen, the complete curved model, in most cases, produced a moment of the opposite sign from that produced by the straight model. This is explained by the fact that the rotary effect was greater than the linear effect. The results of the experiments without a netting (for the complete model) are not given on the graph in a complete form, since they would only obscure the diagram. However, it is readily seen that the curves $R_{\Sigma M} = f(\beta_o)$ for the tests without a netting slope slightly more than the analogous curves of the tests with a netting, and the values

of $R_{\Sigma M}$, at large angles of attack ($\beta_o = 10^o$ to 14^o), are larger in absolute magnitude than the analogous values of $R_{\Sigma M}$ for the tests with a netting.

We are not considering the velocity gradient as the sole cause of this very insignificant deviation. We must bear in mind the fact that, in the presence of the netting, the flow behind it becomes turbulent* to a much greater degree than it is when the netting is absent. Moreover, we must assume that in the flow obtained there are probably present local turbulence, vortices, etc., which no doubt must change to some extent the character of the streamlined flow. Next year we propose to carry on more detailed investigations of the effect of the gradient and the netting on the results of curved model tests.**

Therefore, avoiding criticism and qualitative comparison of the results of tests with a netting and without a netting, we worked up the results of each variant independently to the end.

The results of the tests on the lateral force are given in figure 27 in the form of coefficients of R ($R_{\Sigma z_1}$ is the curved model; R_{z_1}, the straight model). These coefficients are determined by the coefficients of the lifting

*The effect of the turbulent flow is shown very characteristically in the result of curved model tests on drag (see below).

**At first we wanted to exclude the influence of turbulence and nonaxial flows by carrying out the tests with a netting of constant mesh T, in order to compare the obtained results with tests made without a netting. But, owing to the lack of time, we were obliged to give up these tests. From the results of tests with a netting of constant mesh, it would have been possible, with a sufficient degree of probability, to find the values $R_{\Sigma M}$ and $R_{\Sigma z_1}$ that are free from the influence of turbulence and nonaxial flows, making use of the following obvious correlations:

$$R_{\Sigma M} = (R_{\Sigma M})_o \frac{(R_{\Sigma M})_t}{(R_{\Sigma M})_T}$$

where the subscript O refers to the test in free flow, and the subscripts t and T refer to the tests with a netting of variable and constant mesh.

force R_Z and the drag R_x by means of the well-known expression:

$$R_{Z_1} = R_Z \cos \beta_0 + R_x \sin \beta_0 \qquad (47)$$

The first thing immediately noticeable in figure 27 is the fact that, in a large majority of the cases, the tests with the netting gave larger values of $R_{\Sigma Z_1}$ than the tests without the netting.

The results of tests on drag, which, in this work, are of entirely secondary importance, will be discussed below.

It should be mentioned that, in calculating the coefficients of R, the aerodynamic forces and moments referred to the square of the velocity v_0 on the tunnel axis. In the tests with the netting, the velocity was determined in accordance with the readings on the speed control device, making use of those adjustments with which we dealt while investigating the field behind the netting.

5. CORRECTIONS TO THE EXPERIMENTS

The basic correction, introduced when the experiments were worked up, was the correction for the difference in the model curvature which must occur while passing from one angle of attack to another and which we discussed in detail on page 5. This correction was made in the results of the tests on the moment and force according to different methods, for which reason we shall examine each case separately.

a) Correction to the Moments

We have already seen, in figure 18, that the curved axis of the model, constructed with $R_0 = 2.325$ m and $\beta_0 = 0^\circ$, when the model is installed in the tunnel at the angle of attack $\beta_0 = 0$, has a somewhat larger degree of curvature than the axis of our model ($R_0 = 2.325$ m, $\beta_0 = 8^\circ,51'$). This is especially noticeable in the stern of the model, where the tail surfaces are located. The nose parts of both axes merge.

Consequently, the stern of our model, provided with tail surfaces, when $\beta_o = 0^o$, forms a somewhat smaller local mean angle of attack with the flow than would have been formed by a model constructed according to $R_o = 2.325$ m and $\beta_o = 0^o$. When the model is installed at $\beta_o = 0^o$, the difference between these angles is $\Delta\beta_o = 0.258^o$ (0^o 15.5').

Consequently, the true angle of attack of the stern may be obtained by turning our model counter-clockwise (according to fig. 18) at the positive angle $\Delta\beta^o = 0.258^o$.

Naturally, at the other angles of attack, the correction will decrease and, with β^o (set), it will be equal to zero. Thus, the true mean angle of attack of the stern will be:

$$\beta_{true} = \beta_{o\,set} - \Delta\beta_o \qquad (48)$$

However, since the maximum magnitude of $\Delta\beta_o$ is very small, we considered it entirely possible to regard the change of $\Delta\beta_o$ from $\beta_{oset} = 0$ to $\beta_{oset} = 8^o51'$, and higher (until $\beta_{oset} = 14^o$) as rectilinear. This change is shown in figure 28.

Now, let us turn to figure 26. We see that at 1^o angles of attack, the moment of the hull with gondola almost everywhere has the opposite sign from that of the moment of the hull with tail surfaces, and that in most cases it is larger than the latter in absolute value.

Thus, it becomes clear that the negative moment of the hull with tail surfaces is due mainly to the effect of the tail surfaces, the moment of which must be considerably larger in absolute magnitude than the moment of the bare hull.

Therefore, it was decided to introduce the correction for $\Delta\beta_o$ (forumla 48) only in the value of the tail surface moment of the curved model. But there is no basis for assuming that the above-examined difference in the curvature of the stern of the models, constructed with $R_o = 2.325$ and $\beta_o = $ var., will exert a perceptible influence on the moment of the bare hull, since the moment of the latter is produced, principally, by the nose (tip-

ping moment)*. But, according to figure 18, the nose parts of all the models, constructed with $R_o = 2.325$ and β_o = var., merge.

The correction was introduced in the following manner: the magnitude of the coefficient of the tail surface moment was calculated as the difference in the coefficients of the moment of the hull with tail surfaces and of the bare hull; the correction to the set angle of the tail surfaces was introduced according to formula (48), and the results obtained were again combined with the coefficients of the bare-hull moment, which remain unchanged.

b) Correction to the Lateral Forces

The fact that, according to figure 27, the lateral-force values for the bare hull are of the same sign as the lateral forces of the hull with tail surfaces, enables us to assume that both the stern of the curved hull and the tail surfaces exerted an equal influence on the magnitude and sign of the lateral forces. This made it possible and correct to introduce the corrections according to formula (48) to the values of the coefficients of $R_{\Sigma Z_1}$ of the complete model, without separating it into hull and tail surfaces, as was done in the case of the moments.

c) Other Corrections

In working up the tests on R_{Z_1} of the straight model, it was found (as is almost always the case) that the curve $R_{Z_1} = f(\beta_o)$ does not go through zero when $\delta = 0$; this is caused by the nonaxial flow which is produced by the support and the streamlined fairing of the cross member. This circumstance was discounted by the fact that the scale of β_o was displaced in such a way that, when $\beta_o = 0$ and $\delta = 0$, $R_{Z_1} = 0$. The scale of β_o was also displaced in this manner when the tests on $R_{\Sigma Z_1}$ and R_{Σ_X} of the curved model were worked up, since the support and the streamlined fairing were the same.

*This conclusion is also corroborated by the circumstance that the moment of the bare curved hull changes the sign at small angles β_o, i.e., at the point where the local angle of attack of the nose becomes negative.

All the other very small corrections did not differ in any respect from the usual corrections introduced in the case of standard experiments (coefficient of the field, influence of the gradient of static pressure, resistance of the support, etc.). Therefore, we are not discussing them here.

The curves in figures 26 and 27 contain all the corrections indicated.

6. CALCULATION OF THE ROTARY DERIVATIVES

The rotary derivatives of the moment, lateral force and drag were calculated according to the formulas (38), derived on page 32 of Part I (Technical Memorandum No. 829), in which formulas R_0 was assumed to be equal to 2.325 m.

Figure 29 shows the rotary derivatives of the moment $\left[\frac{1}{v_0}\frac{\partial M_y}{\partial \omega_y}\right]$ as a function of the angle of attack β_0 for the different rudder angles of deviation δ and for the bare hull with gondola and without gondola. As should have been expected, the rotary derivatives obtained for the bare hull were much smaller than those obtained for the hull with tail surfaces. The peculiar bend upward of the curve $\left[\frac{1}{v_0}\frac{\partial M_y}{\partial \omega_y}\right]$ of the hull without car was due to the sudden bend downward of the curve $R_{\Sigma M} = f(\beta_0)$ of the hull without car (fig. 26).

The curves $\left[\frac{1}{v_0}\frac{\partial M_y}{\partial \omega_y}\right] = f(\beta_0)$ for the hull with tail surfaces (fig. 29) flow in such a tangled and, at the first glance, irregular bundle* that, according to it,

*This circumstance made it impossible to construct in figure 29 the curves $\left[\frac{1}{v_0}\frac{\partial M_y}{\partial \omega_y}\right] = f(\beta_0)$ for all the rudder angles of deviation; it would have confused the diagram still more.

except for the increase, in general, of $\left[\frac{1}{v_0}\frac{\partial M_y}{\partial \omega_y}\right]$ with the angle of attack, it is very difficult to make other quantitative conclusions. However, if we construct the values $\left[\frac{1}{v_0}\frac{\partial M_y}{\partial \omega_y}\right]$ as a function of the rudder angle of deviation and on a considerably magnified scale (fig. 32), immediately we notice some regularity; this is especially clearly evident at small angles β_0 and is confirmed both by experiments with the netting as well as without the netting. To begin with, this regularity consists in the presence of two sufficiently pronounced maxima* on the majority of the curves, and secondly, in the large decrease of the rotary derivative with large angles δ. It seems to us that the reason for such sinuosity of these curves should be sought in the somehow regularly varying mutual influence of the rudder, the compensator and the stabilizer.

On the basis of figure 32, we may say that the condition, which, in the previous papers on curvilinear flight, assumes that the moment rotary derivatives are independent of the rudder angle of deviation, must be admitted as being correct in the first approximation, since the maximum deviations of the values of the rotary derivative at the different δ (from 0 to from 25° to 30°) from its value when $\delta = 0$ do not exceed, in the majority of cases, from 5 to 6 percent. However, when we examine the variation, with the angle of attack of the bare hull rotary derivative, we find that the condition, which assumes that the hull rotary derivative is independent of the angle of attack, must be regarded as entirely unsatisfactory, since the difference in the values of $\left[\frac{1}{v_0}\frac{\partial M_y}{\partial \omega_y}\right]_{hull}$ when $\beta \neq 0$ and when $\beta = 0$, amounts to ~ 60 percent.

Figure 31 shows the variation, with reference to the angle of attack β_0, of the lateral force rotary derivatives both for the hull with tail surfaces as well as for the bare hull.

It is interesting to note that the condition assumed by the English, namely, that the hull rotary derivative is

*The second maximum is larger than the first.

constant with reference to the angle of attack, and that the hull rotary derivative is equal to 0.1 m, where m is the mass of air displaced by the model, is not fulfilled (the difference amounts to 100 percent).

This will be seen from a comparison of the curves $\left[\frac{1}{v_0}\frac{\partial Z_1}{\partial \omega_y}\right]_{hull}$ with the straight line $\left[\frac{1}{v_0}\frac{\partial Z_1}{\partial \omega_y}\right]_{hull} = 0.1\ m$, plotted on the same diagram.

The curves representing the variation of the lateral force rotary derivative of the hull with tail surfaces, similarly to the curves of figure 29, are shown in the form of a somewhat tangled, although more regular, bundle. The fundamental regularity of the change of $\left[\frac{1}{v_0}\frac{\partial Z_1}{\partial \omega_y}\right]$ appears sufficiently clearly in figure 33, where $\left[\frac{1}{v_0}\frac{Z}{\partial \omega_y}\right]$ are given (analogously to fig. 32) as a function of the rudder angle of deviation δ. This regularity is apparent from the fact that, when the angle δ is increased, the rotary derivatives tend to decrease at small angles of attack, and tend to increase at large angles of attack. It should be mentioned, in particular, that, in all the cases, the lateral force rotary derivatives were larger during tests with a netting than during tests without a netting. This difference sometimes amounts to 12 percent.

Now, let us compare the values of the rotary derivatives obtained by the method of curved models and by the oscillation method. This comparison is shown in figure 30.

As will be seen, the values of the moment rotary derivative, obtained by the method of curved models, were everywhere smaller than the values of the rotary derivative determined by the oscillation method. Besides, the peculiar bend in the curve, obtained by the oscillation method, did not appear in the curve, constructed by the aid of the curved model method.

The reason for these divergences, amounting to 10 percent, must be sought in the following:

1) The rotary derivatives were determined by the oscillation method in the NK-1 tunnel, in which, as a rule, the tests sometimes differ considerably from those carried out in the T-3 tunnel.

2) The model tested in the NK-1 tunnel had a somewhat greater relative elongation than the curved model, the elongation of which was exactly similar to the full-size ship.

3) The theory underlying the determination of the rotary derivative contains, according to the damped oscillation records, many merely approximately correct assumptions and, moreover, the experimental results are considerably distorted, due to the imperfection of the equipment used for recording the damping* (it is true that recently we have greatly improved the method of recording damped oscillations and of working up the data).

4) The origin of the enigmatical bend on the curve

$$\left[\frac{1}{v_0}\frac{\partial M_y}{\partial \omega_y}\right]$$ obtained by the oscillation method,

is explained, in our opinion, by the influence on the tail surfaces of vortices that get detached from some parts of the apparatus located in the flow. The tail surfaces immediately become blanketed with these parts at the model angles of attack of from 5 to 8 degrees, that is to say, exactly at those angles at which the indicated bend occurs.

It is self-evident that the close coincidence of the lateral force rotary derivatives, obtained in figure 30, is purely accidental since, in the case of the damped oscillation method, the lateral force rotary derivative was calculated according to the rotary derivative of the moment (for which no coincidence was obtained) by the aid of various assumptions of extremely low probability (for example $\left[\frac{1}{v_0}\frac{\partial M_y}{\partial \omega_y}\right]_{hull}$ = const.; $\left[\frac{1}{v_0}\frac{\partial Z_y}{\partial \omega_y}\right]_{hull}$ = 0.1 m)

*Concerning these imperfections, see our work on radii of turn.

the incorrectness of which has already been ascertained.

7. RESULTS OF THE EXPERIMENTS BASED ON THE DETERMINATION OF THE DRAG

In testing the curved model on drag, we first of all discovered a very great difference between the results of tests with a netting and without a netting. During tests with a netting, the coefficients of drag were found everywhere to be from 35 to 70 percent smaller than the corresponding coefficients obtained in the tests without a netting. Apparently, this difference is to be attributed, in the first place, to the artificial turbulence of the flow due to the netting, which gives the boundary layer of the model a structure more closely resembling the structure obtained with high Reynolds Numbers and, in the second place, the difference is to be attributed to the possible considerable drop in the statical pressure along the tunnel behind the netting.

The very interesting problem concerning the possibility of obtaining, by the aid of artificial turbulence in the flow, an artificial increase in the Reynolds Number, can and ought to be the subject of special earnest investigation.

Figure 34 shows the relations to β_0 of the coefficients of drag of the curved and straight models. These curves are given only for the rudder angle of deviation $\delta = 0$. The remaining wind tunnel tests, although they have been carried out and worked up, are here of much less interest in principle and, therefore, are not shown.

Figure 34 also shows the relation to β_0 of the rotary derivative of the drag $\left[\frac{1}{v_0}\frac{\partial X}{\partial \omega_y}\right]$ calculated by us according to the first formula of the system (38) (page 32 of Part I, Technical Memorandum No. 829), also for $\delta = 0$. This derivative was calculated only according to the wind tunnel tests without a netting, since we did not have any tests of the straight model in a flow with the

same degree of turbulence as was created by the netting with variable mesh*.

8. CONSTRUCTION OF THE NOMOGRAMS OF THE RADII OF TURN

COMPARISON OF THE NOMOGRAMS WITH FREE FLIGHT TESTS

AND WITH RESULTS OF PREVIOUS TESTS

After determining the relations of the rotary derivatives of the moments and lateral forces to β_o and δ, it became possible to construct the nomograms that are analogous to those in figure 16. The values are the reverse of the radius of turn, with which radius there is established, for the various β_o and δ, the equilibrium either of the forces or of the moments. These values were calculated according to the well-known expressions (reference 1):

According to the condition of equilibrium of forces

$$\left.\begin{aligned} \frac{1}{R_o} &= \frac{R_{z_1}}{m \cos \beta_o - \left[\frac{1}{v_o} \frac{\partial Z_1}{\partial \omega_y}\right]} \\ \text{According to the condition of equilibrium of moments} \quad \frac{1}{R_o} &= \frac{R_{m_y}}{\left[\frac{1}{v_o} \frac{\partial M_y}{\partial \omega_y}\right]} \end{aligned}\right\} \quad (49)$$

*It was possible to work up the results of the wind tunnel tests on the moments and the lateral force, making use of the tests with and without the netting simultaneously (curved and straight models), due to the fact that, according to the series of foreign investigation, the magnitudes of the lifting forces and moments depend but little on the degree of turbulence in the flow. Thus, on the magnitudes of the lateral forces, calculated according to formula (47) the differences in the values of $R_{\Sigma X}$, obtained in tests with and without a netting, must show an insignificant effect because, in the formula indicated $R_{\Sigma X}$ is multiplied by the sine of the small angles.

These nomograms, constructed according to the wind tunnel tests with and without a netting, are shown in figures 35 and 36. On the left of the diagrams are given the hyperbolical scales, which enable us to obtain the values, in meters, of the radii of turn R_o for the full-scale airship.

As will be seen from these nomograms, the points on the straight line $\frac{1}{R_o} = f(\beta_o, \delta)$ in figure 36 are particularly well placed, that is to say, according to the tests without a netting. This partly leads us to surmise that they are more reliable as compared to the tests with the netting. The fact that the straight line $\frac{1}{R_o} = f(\beta_o, \delta)$ passed through zero is particularly valuable, since this line did not go through zero before. (See fig. 16.) The degree of reliability of our present tests is thereby greatly increased.

Some deviations of the points from the straight line $\frac{1}{R_o} = f(\beta_o, \delta)$, which occur (figs. 35 and 36) mainly at large rudder angles of deviation, in our opinion, are due either to the influence of the compensator or to the loss of effectiveness on the part of the rudder.

There is no basis for attributing these deviations, in a large measure, to experimental errors, since such deviations, in the same direction, occur on both curves (figs. 35 and 36). This is shown especially clearly in figure 37, where a comparison is made of the relations of $\frac{1}{R_o} = f(\beta_o, \delta)$ on the basis of the results of the present tests and the results of tests by the aid of the damped oscillation method and according to free-flight tests. As will be seen, the general direction of the curves coincides well enough: the deviations (general) seldom amount to 10 percent.

At first glance, it might seem that the results of the old tests by the aid of the oscillation method are in better agreement with the free-flight tests than the re-

sults of the present tests. However, this phenomenon is purely accidental: we have to assume that, in free-flight tests, errors may occur which lie within the 10-percent limit.*

Figure 38 shows a comparison of the relations of the radii of turn to the rudder angle of deviation, according to our various experiments.

We cannot discuss in detail the causes of all the divergencies (of a qualitative and quantitative order), since, for this purpose, it is necessary to have a considerably larger number of experiments than we have in this work.

Let us mention one fact which we think is interesting. In figure 36, when $\delta = 0$, the curves of the equilibrium of the moments and forces intersected at the origin of the coordinates ($\beta_0 = 0$, $R_0 = \infty$, rectilinear motion) as well as at some other point $\left(\frac{1}{R} = 0.0925\ m^{-1}\right.$ $\left.R_0 \text{ full scale} = 700\ m\right)$. A similar fact was noted also in the old tests. (See fig. 16.)

This circumstance indicates that, when the rudder is neutral, the given airship evidently can fly along a circle with a very large radius. It is interesting to note that this fact is confirmed by several free-flight tests made abroad.

By using the graphs 35 and 36 and also the figures 26, 27, 29, and 32 and the rotary derivatives of drag, not entered here, it was found possible to construct three graphs that are of great theoretical interest (figs. 39, 40, and 41).

Graphs of this kind should be very useful in the aerodynamic calculation of airship designs.

These graphs show, as a function of $\frac{1}{R_0}$ of the model**

*It was found that, in free-flight tests, the tail surfaces are displaced somewhat forward, as compared to the original position. This fact was not taken into account in the tests.

**I.e., as a function of the magnitude, proportional to the angular velocity ω_y.

the values of the nondimensional coefficients of the total moments, lateral forces, and drags ($C_{\Sigma M}$, $C_{\Sigma Z_1}$, $C_{\Sigma X}$) acting on the airship in balanced flight along circles of different radii, as well as their components, i.e., coefficients of the forces and moments resulting from the linear as well as the rotary displacements:

$$C_{m_y},\ C_{z_1},\ C_x \quad \text{and} \quad C_{m_\omega},\ C_{z_{1\omega}},\ C_{x_\omega}$$

These curves are obtained for the states of equilibrium of flight along circles $\left[\frac{1}{R_o},\ \beta_o \text{ and } \delta\right.$, corresponding to the points of the straight lines $\frac{1}{R_o} = f(\beta_o, \delta)$ (figs. 35 and 36) and their ordinates are calculated according to the formulas:

$$C_{m_y} = \frac{2\,R_{m_y}}{\rho\,U};\quad C_{z_1} = \frac{2\,R_{z_1}}{\rho\,S};\quad C_x = \frac{2\,R_x}{\rho\,S} \tag{50}$$

$$C_{m_\omega} = \frac{2\,R_{m_\omega}}{\rho\,U} = \frac{2\omega_y\left[\frac{\partial M_y}{\partial \omega_y}\right]}{\rho U\,v_o^2} = \frac{2\,\frac{1}{R_o}\left[\frac{1}{v_o}\,\frac{\partial M_y}{\partial \omega_y}\right]}{\rho\,U} \tag{51}$$

$$C_{z_{1\omega}} = \frac{2\,R_{z_{1\omega}}}{\rho\,S} = \frac{2\omega_y\left[\frac{\partial Z_1}{\partial \omega_y}\right]}{\rho\,S\,v_o^2} = \frac{2\,\frac{1}{R_o}\left[\frac{1}{v_o}\,\frac{\partial Z_1}{\partial \omega_y}\right]}{\rho\,S} \tag{52}$$

$$C_{x_\omega} = \frac{2\,R_{x_\omega}}{\rho\,S} = \frac{2\omega_y\left[\frac{\partial X_1}{\partial \omega_y}\right]}{\rho\,S\,v_o^2} = \frac{2\,\frac{1}{R_o}\left[\frac{1}{v_o}\,\frac{\partial X_1}{\partial \omega_y}\right]}{\rho\,S} \tag{53}$$

$$C_{\Sigma M} = C_{m_y} + C_{m_\omega};\quad C_{\Sigma Z_1} = C_{Z_1} + C_{Z_{1\omega}};\quad C_{\Sigma X} = C_x + C_{x_\omega} \tag{54}$$

The formulas (50) are the well-known transformations

from the coefficients of R to the nondimensional coefficients of C by expressing R in terms of half the density, the volume U or the midship section S.

The formulas (51), (52), and (53) are obvious and are given in the form of consecutive and very simple transformations (R_o is regarded as variable).

In figure 39, due to the equilibrium of the linear and rotary moments, the magnitudes C_{m_y} and C_{m_w} are equal in magnitude and opposite in sign, which stipulates that $C_{\Sigma M} = 0$ (54).

In figure 40, the magnitude $C_{\Sigma Z}$ is everywhere equal to and opposite in sign to the coefficient of centrifugal force, which coefficient may be calculated as follows:

The coefficient of centrifugal force =

$$= \frac{\frac{m v_o^2}{R_o}}{\frac{\rho v_o^2}{2} S} \cos \beta_o = \frac{2m \cos \beta_o}{\rho R_o S} * \qquad (55)$$

which follows from the equilibrium of all the forces.

Figure 41, can be used as initial data for calculating the loss of velocity in flight along circles of different radii. This can be verified very simply by flight tests.

CONCLUSIONS

In summing up all we have said above, we must admit that the method of curved models, in addition to its very great aerodynamic theoretical vlaue, also have very great practical value. It is superior to the oscillation method in the following points:

*cos β_o occurs due to the fact that the direction of the centrifugal force and the direction of the airship's axis are not perpendicular.

1) The accuracy of the curved model test lies within the limits of accuracy of aerodynamic tests in general, while the accuracy of the oscillation method is very low. This is mainly due to the imperfection of the apparatus used in the oscillation method, and to the considerable number of "ballast" quantities that have to be measured.

2) By the aid of the oscillation method we cannot mea-measure directly the lateral force rotary effects that can be calculated on the basis of assumptions, the considerable discrepancy of which with actual conditions has already been shown.

3) The rotary effects of drag cannot be determined at all by means of the oscillation method.

4) Owing to the accuracy and simplicity of curved model tests, we can investigate the changes in the rotary derivatives with respect to the rudder angle of deviation. In the case of the oscillation method, the changes of the rotary derivatives absolutely lie within the limits of accuracy of the test.

5) By the aid of the method of curved models (when we prepare several models with R_o = var.) we can investigate the change in the rotary derivatives with reference to the angular velocity. However, with the oscillation method this is entirely impossible, since one of the basic assumptions of the latter method is that the rotary derivatives are independent of angular velocity.

6) By the aid of the method of curved models we can study experimentally the distribution of aerodynamic loads in curvilinear flight.

The majority of these merits were corroborated by experiments. The results of experiments carried out according to the method of curved models showed that the relations of $\frac{1}{R_o} = f(\beta_o, \delta)$ are much more regular than in the case of the oscillation method, and that they are in suf-

ficiently good agreement with the results of free-flight tests.

The possibility of making use of one curved model for studying motion along circles of different radii is especially valuable. It considerably simplifies the use of the present method and reduces the cost of its application.

In addition to the errors, indicated in Part I, which are due to the fact that the rotation of circular motion insufficiently conforms to physical laws, and the errors attributable to the contraction and elongation of the arc of the meridional contour, the method also has the following faults:

1) It is necessary to employ gradient devices (particularly a netting) in order to achieve more accurate similarity to curvilinear flight. These devices most likely distort the flow and introduce additional difficulties in the way of obtaining the similarity indicated.

2) It is necessary to produce a special model which is rather complicated in construction.

3) It is necessary to carry on the experiments with particular care and accuracy, since the rotary derivatives are determined by the formulas (38) as differences of the results of experiments which are made at different times and which frequently (for example, in the case of lateral forces) do not differ to any significant degree. Right now we may say with certainly that the accuracy of measurement, for example, of the moment, on the conventional moment apparatus is not sufficiently high.

Next year we propose to endeavor to find a more exact and reliable solution of the problem concerning the influence of the velocity gradient and the presence of the netting on the experimental results than we have given in this paper. It is very probable that the influence of the velocity gradient is very insignificant, and possibly negligible.

In conclusion, we wish to express the hope that the method of curved models may find application not only in

aerodynamic investigations of airships, but also in aerodynamic investigations of other aircraft, as well as in hydrodynamic investigations of naval vessels and submarines.

Translation by Translation Section,
Office of Naval Intelligence,
Navy Department,
Bluma Karp.

REFERENCE

1. Fediaevsky, K. K., and Gourjienko, G. A.: Determination of the Radii and Angles of Turn of an Airship, as a Function of the Rudder Angles of Deviation.

TABLE I

X_1	0	0,025	0.0505	0.1	0.2	0.3	0.4	0.5	0.6	0.7	0.8	0.85	0.9
x_1	- .0505	- .0255	0	.0495	.1495	.2495	.3495	.4495	.5495	.6495	.7495	.7995	.8495
x	- .0505	- .0255	0	.0495	.1495	.2490	.3480	.4660	.5450	.6410	.7380	.7845	.8310
z'	.00055	.00027	0	.00053	.00485	.01345	.0264	.0435	.0647	.0899	.1190	.1350	.1517
y_1	0	.0439	.0582	.0751	.0926	.0992	.0997	.0960	.0882	.0770	.0515	.0322	0

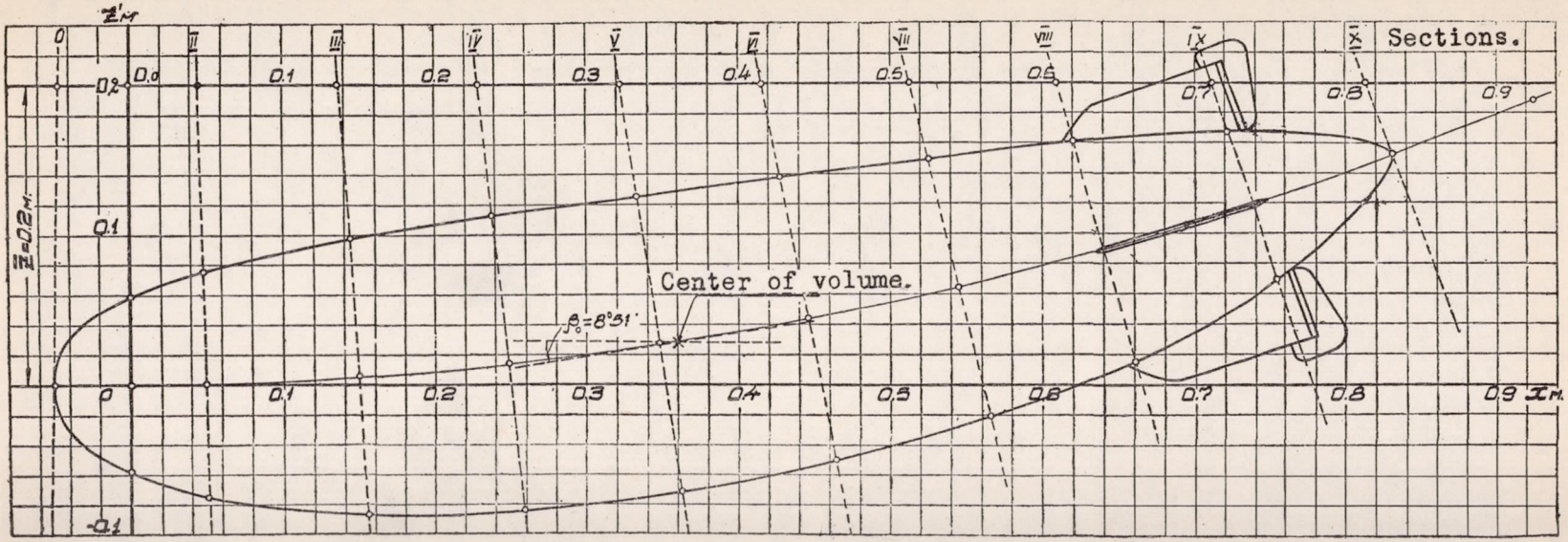


Figure 17.- Construction of the profile of the curved model of the V-2 dirigible (view from above). According to the simplified method.

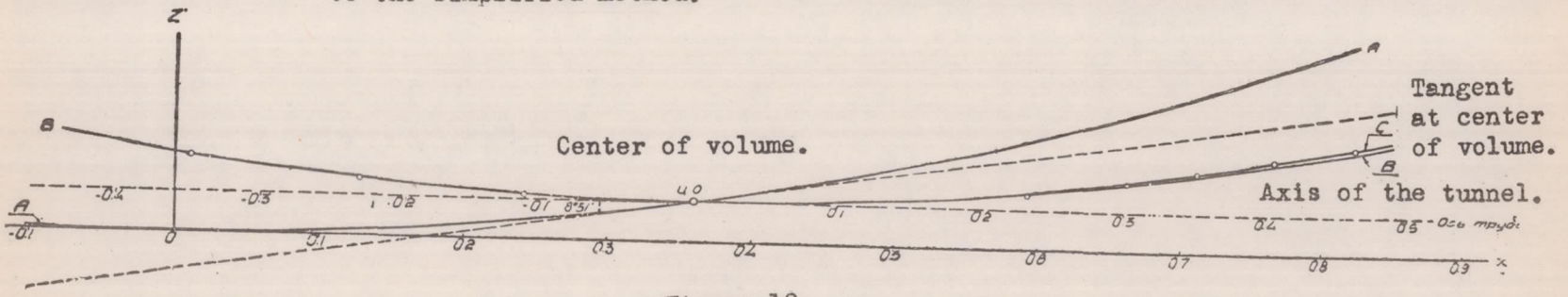


Figure 18.

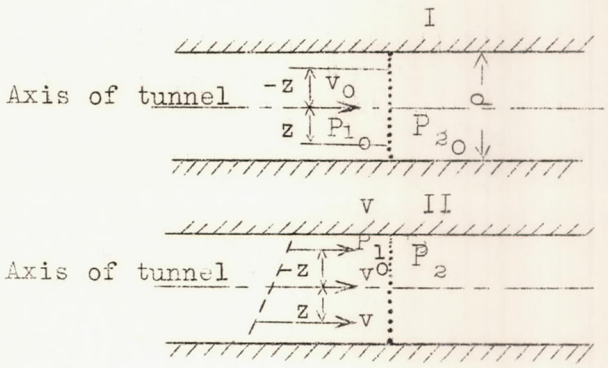


Figure 19.

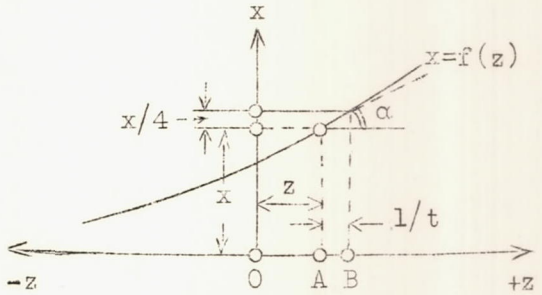


Figure 20.

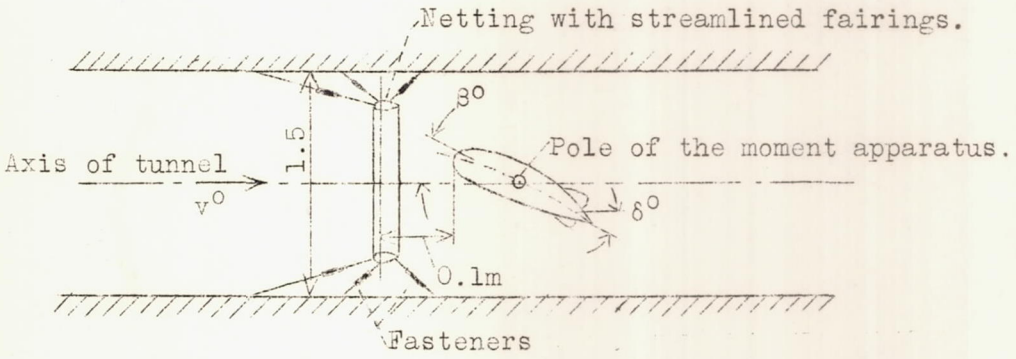


Figure 23.- Arrangement of the curved V-2 model behind the variable mesh netting during wind tunnel tests on the moment in the working part of the T-3 tunnel.

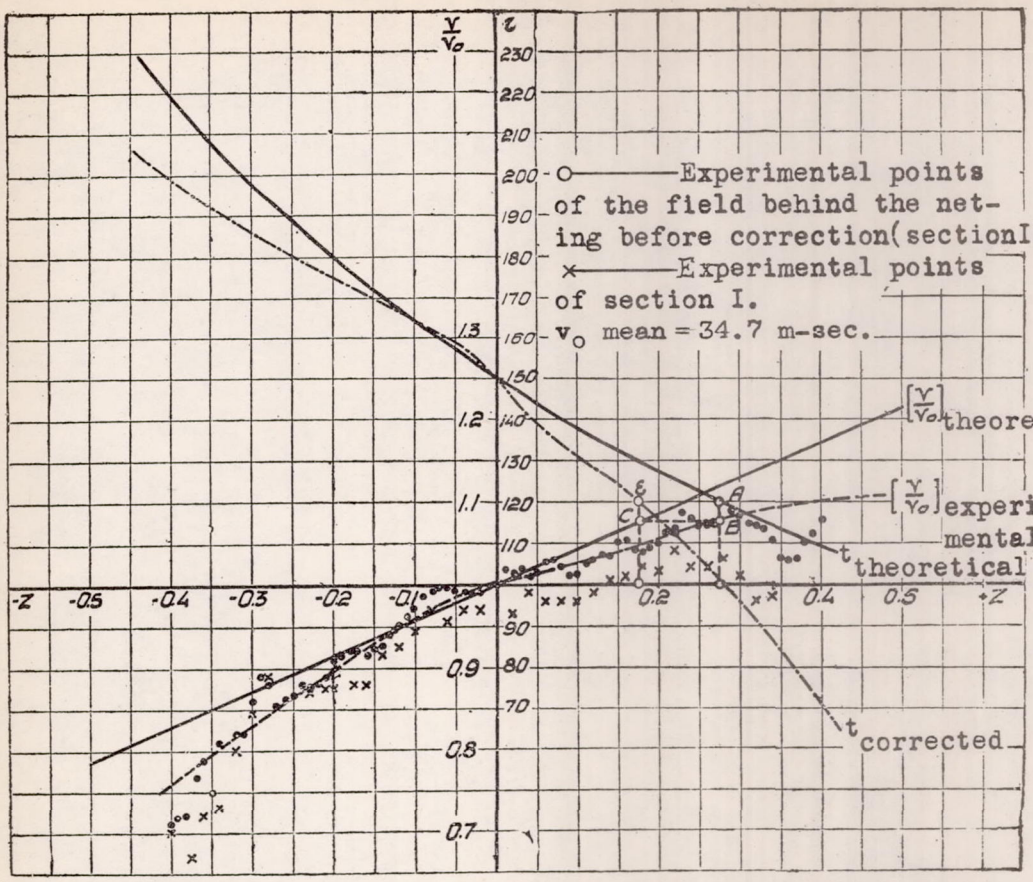


Figure 21.- Investigation of the field of velocities behind the variable mesh netting $t_{theoretical}$ (before correction).

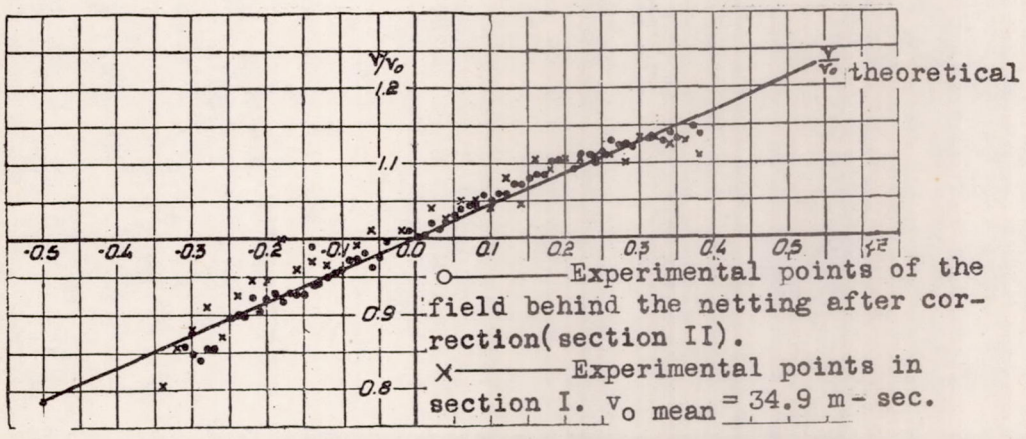


Figure 22.- Investigation of the field of velocities behind the netting of variable mesh (after correction).

$t_{corrected}$

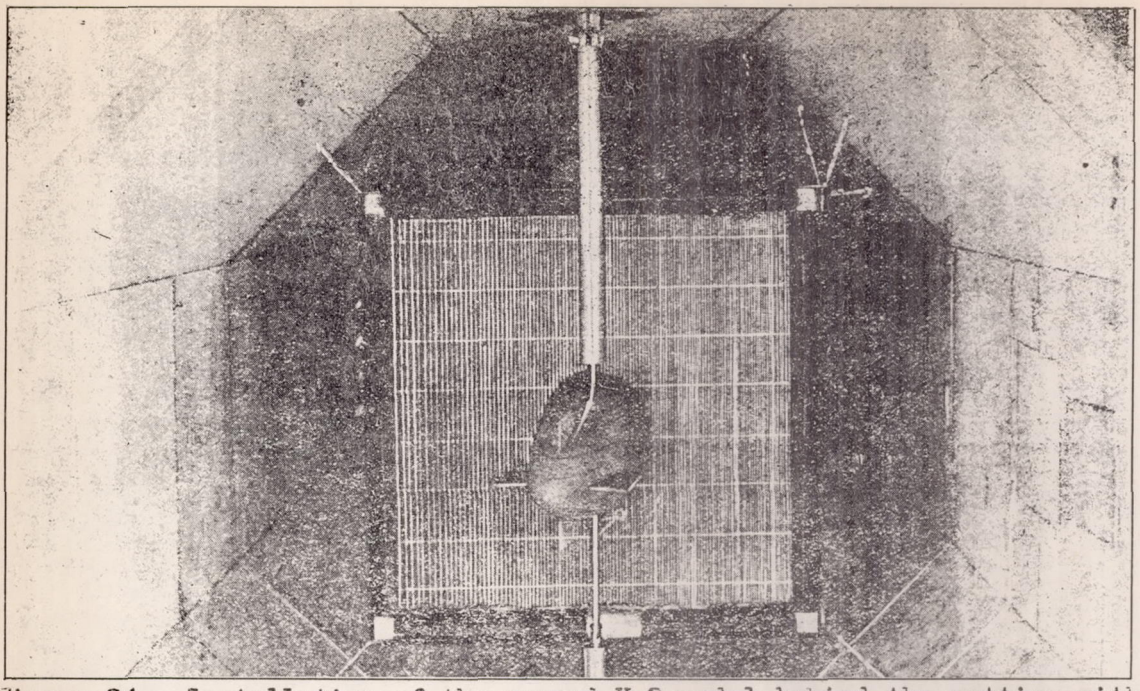


Figure 24.- Installation of the curved V-2 model behind the netting with variable mesh in the T-3 tunnel.(View from the stern)

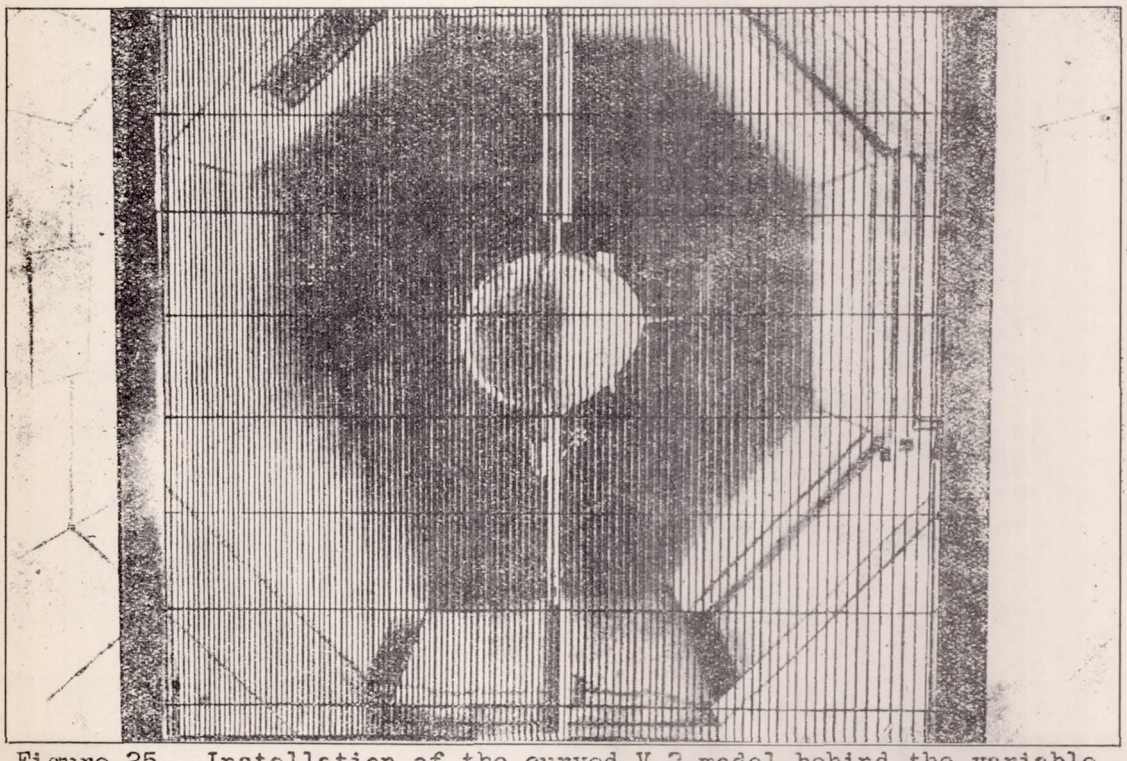


Figure 25.- Installation of the curved V-2 model behind the variable mesh netting in the T-3 tunnel. (View from the nose through the netting).

a, hull and hull with gondola.
b, hull with tail surfaces (straight model).
c, hull with tail surfaces (curved model).

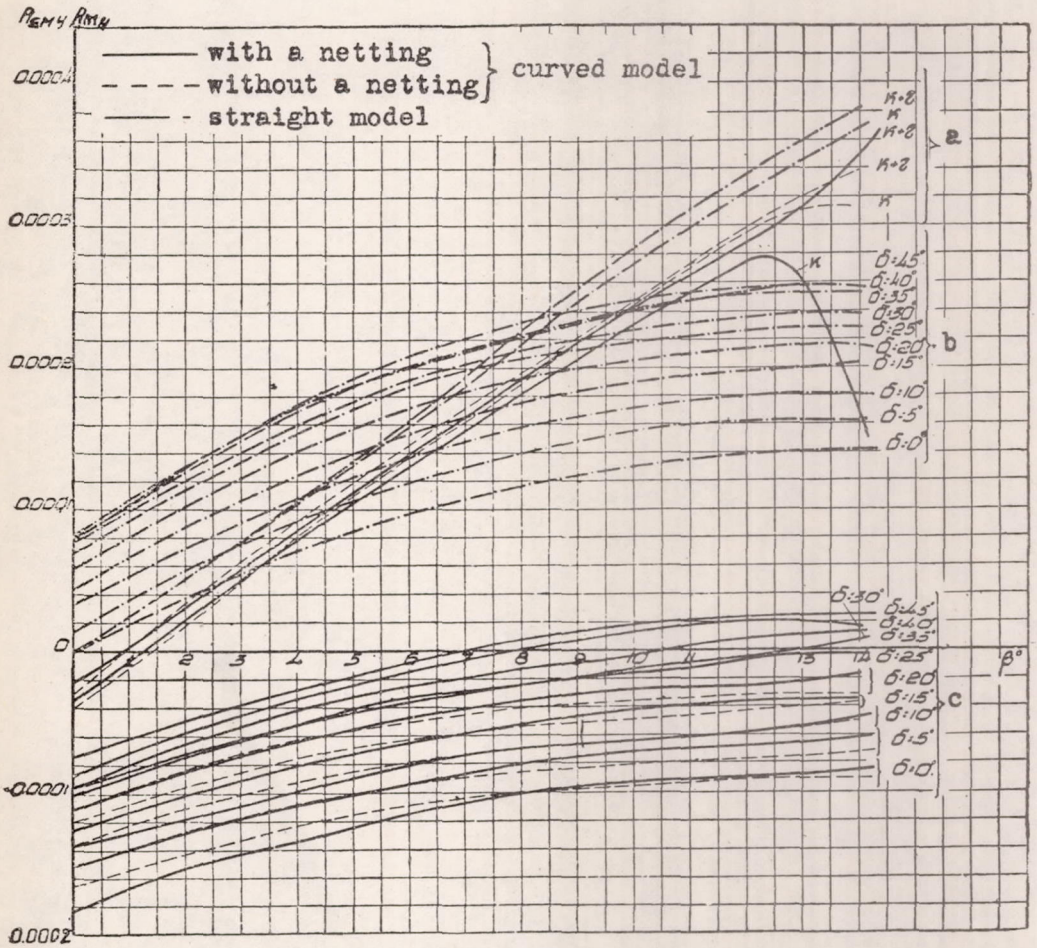


Figure 26.- Values of the coefficients of $R_{\Sigma M}$ and R_{m_y} of the aerodynamic moment of the curved and straight V-2 models as a function of the angle of attack β.

——— Experiment with netting. } curved model.
– – – – Experiment without netting. }
——— - Straight model.

a, hull with tail surfaces (curved model).
b, hull with tail surfaces (straight model).
c, hull and hull with gondola.

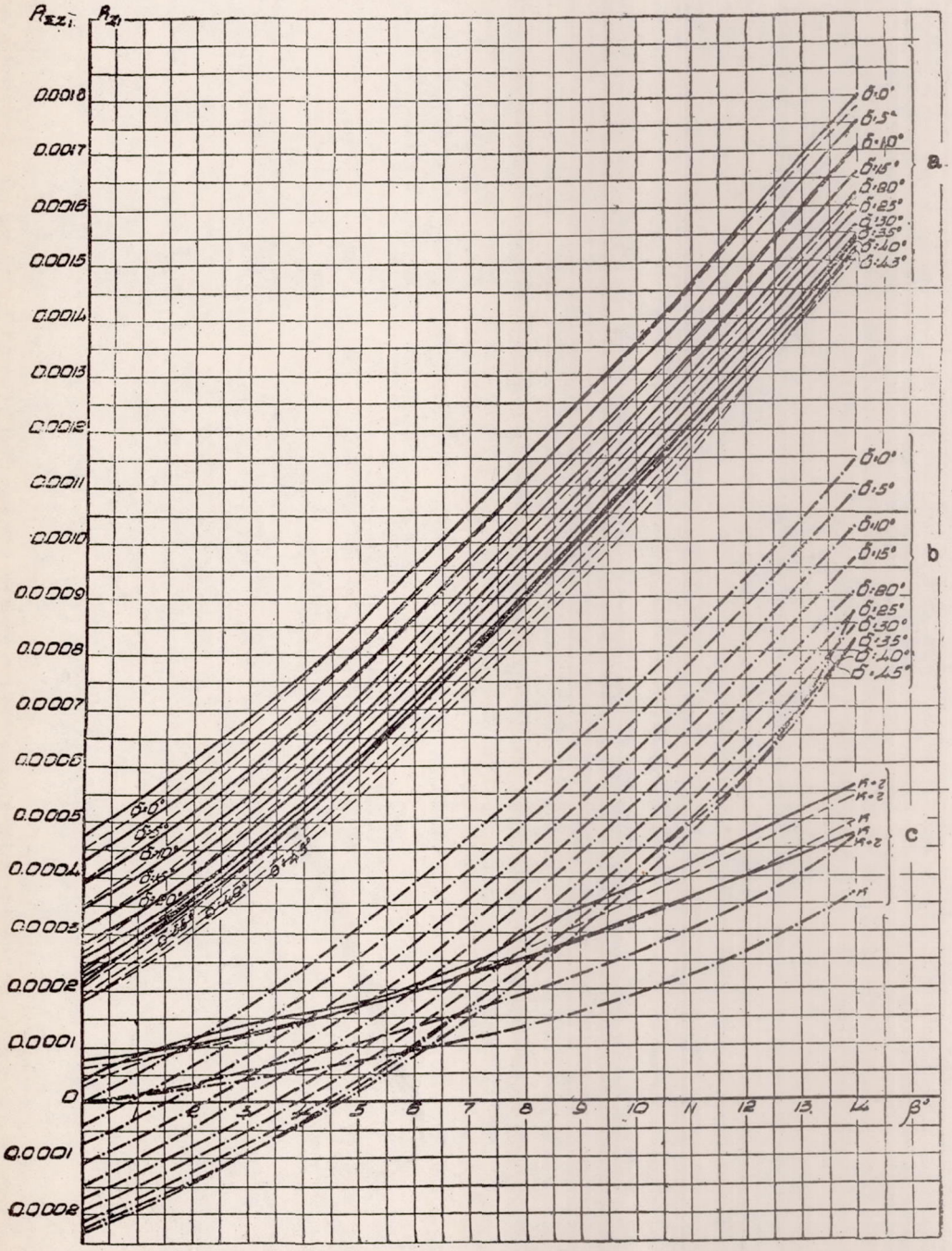


Figure 27.- Values of the coefficients of $R_{\Sigma Z_i}$ and R_{z_i} of the lateral forces of the curved and the straight V-2 models as a function of the angle of attack β_o.

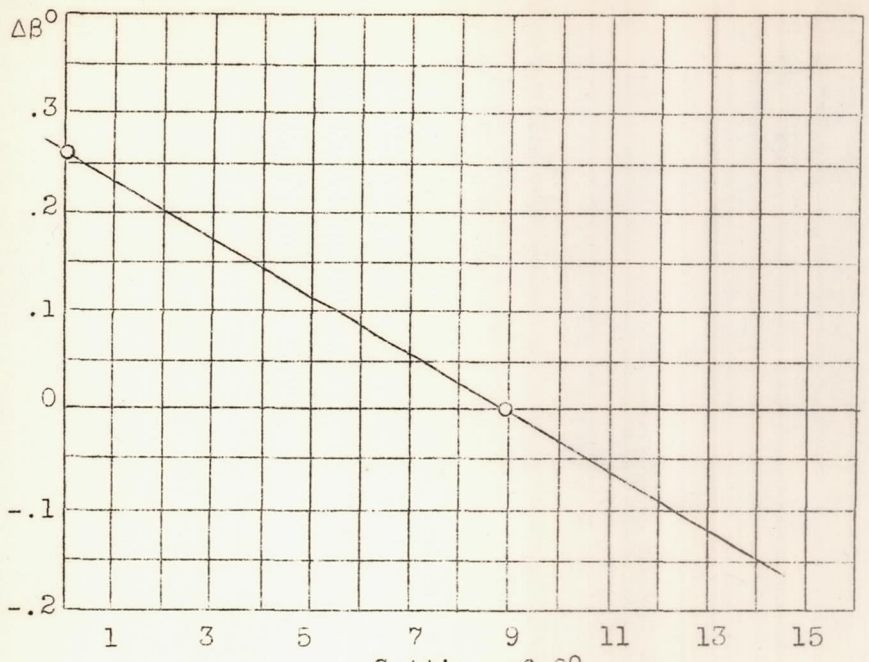


Figure 28.

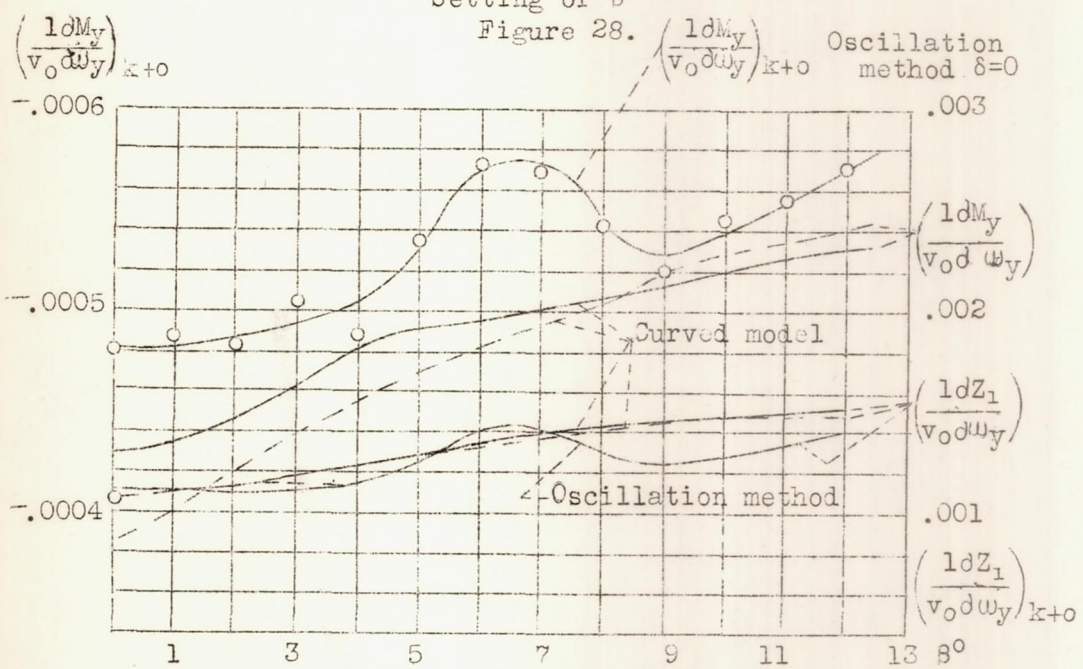


Figure 30.- Change of the rotary derivatives of the forces $\left(\frac{1}{v}\frac{dZ_1}{d\omega_y}\right)_{k+o}$ and of the moment $\left(\frac{1}{v_o}\frac{dM_y}{d\omega_y}\right)_{k+o}$ for the complete V-3 dirigible $\left(\frac{1}{46.48}\text{ full-scale size}\right)$ with reference to the angles of attack β_o when $\delta=0$.

———— with netting
– – – – – – without netting

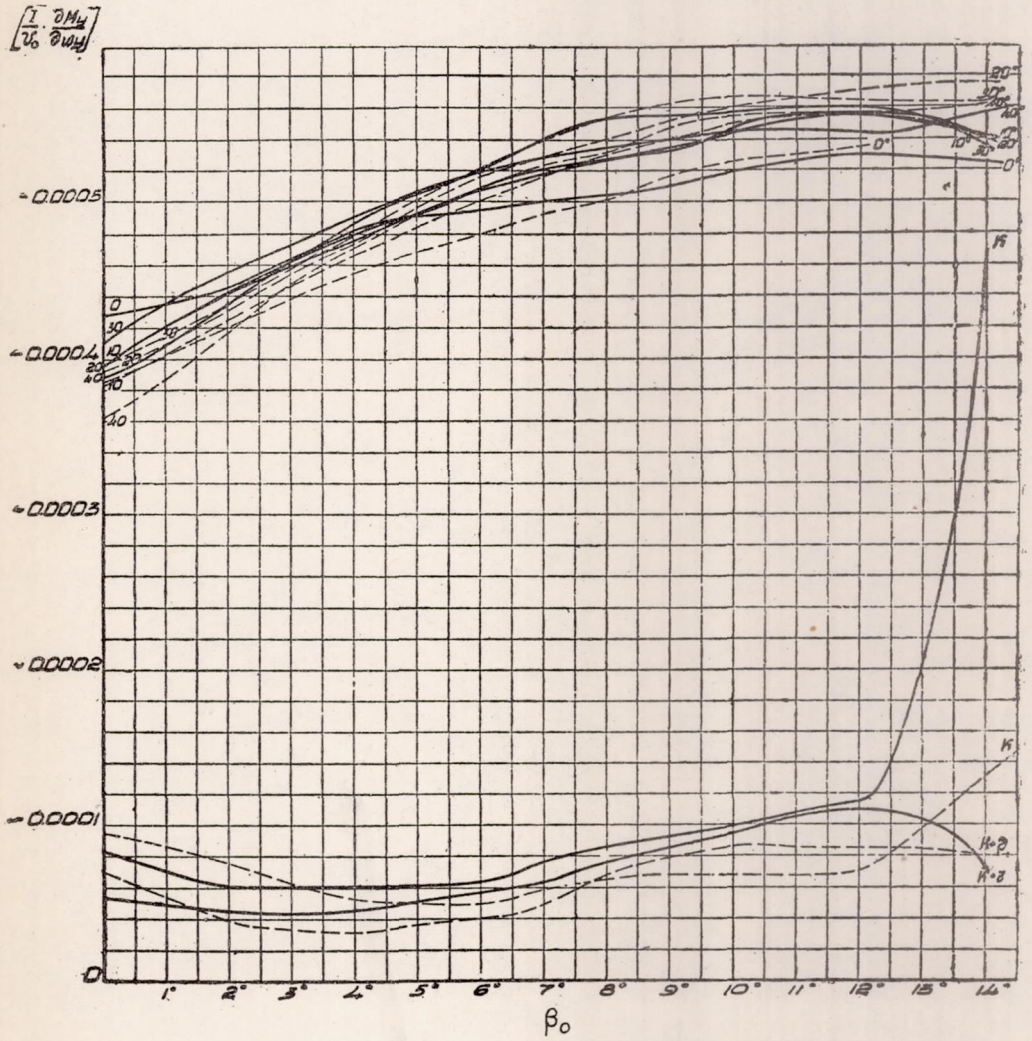


Figure 29.- Values of the moment rotary derivatives of the V-2 model as a function of the angle of attack β_0. (Curved model tests).

——— experiments with variable mesh netting.
– – – – experiments without variable mesh netting.

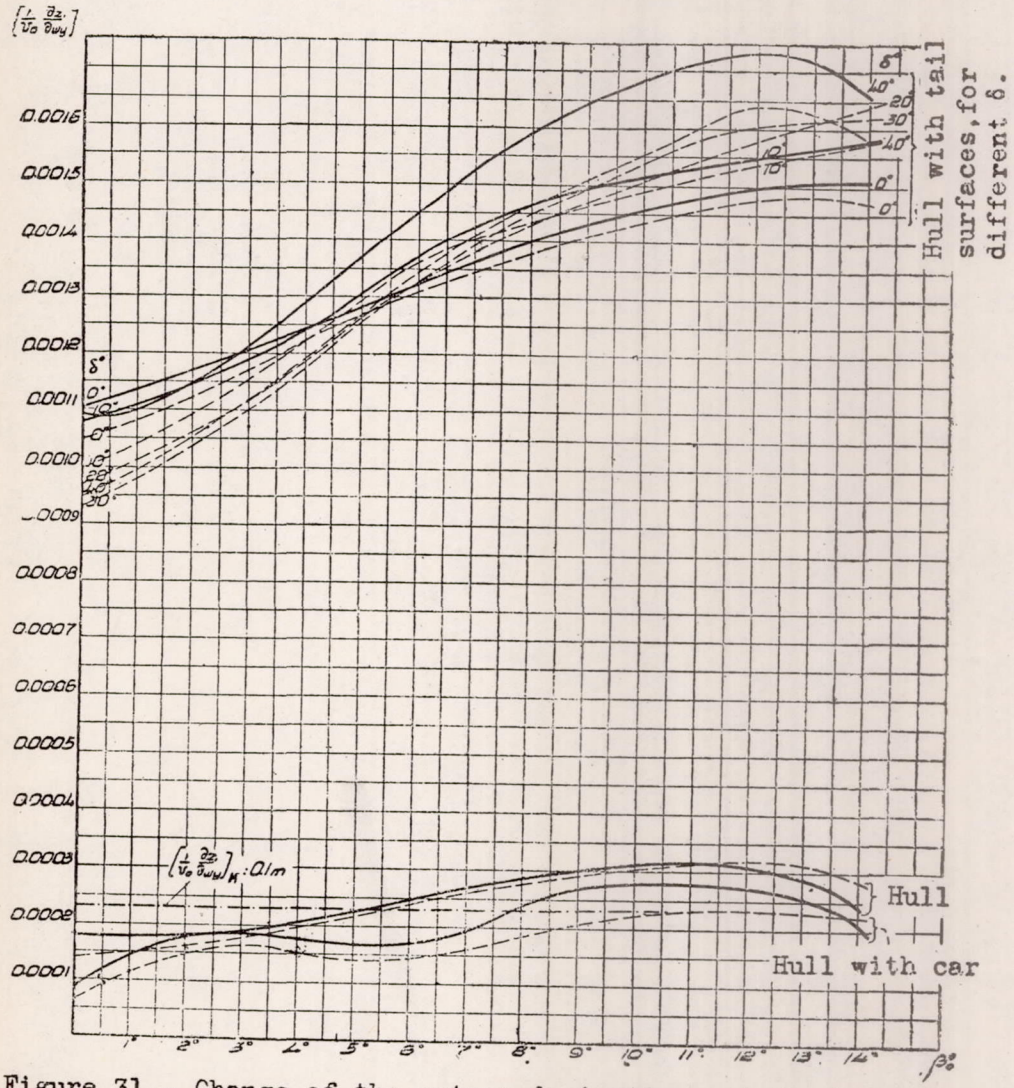


Figure 31.- Change of the rotary derivatives of the lateral aerodynamic forces with reference to the angle of attack β_0 according to the tests with the curved V-2 model.

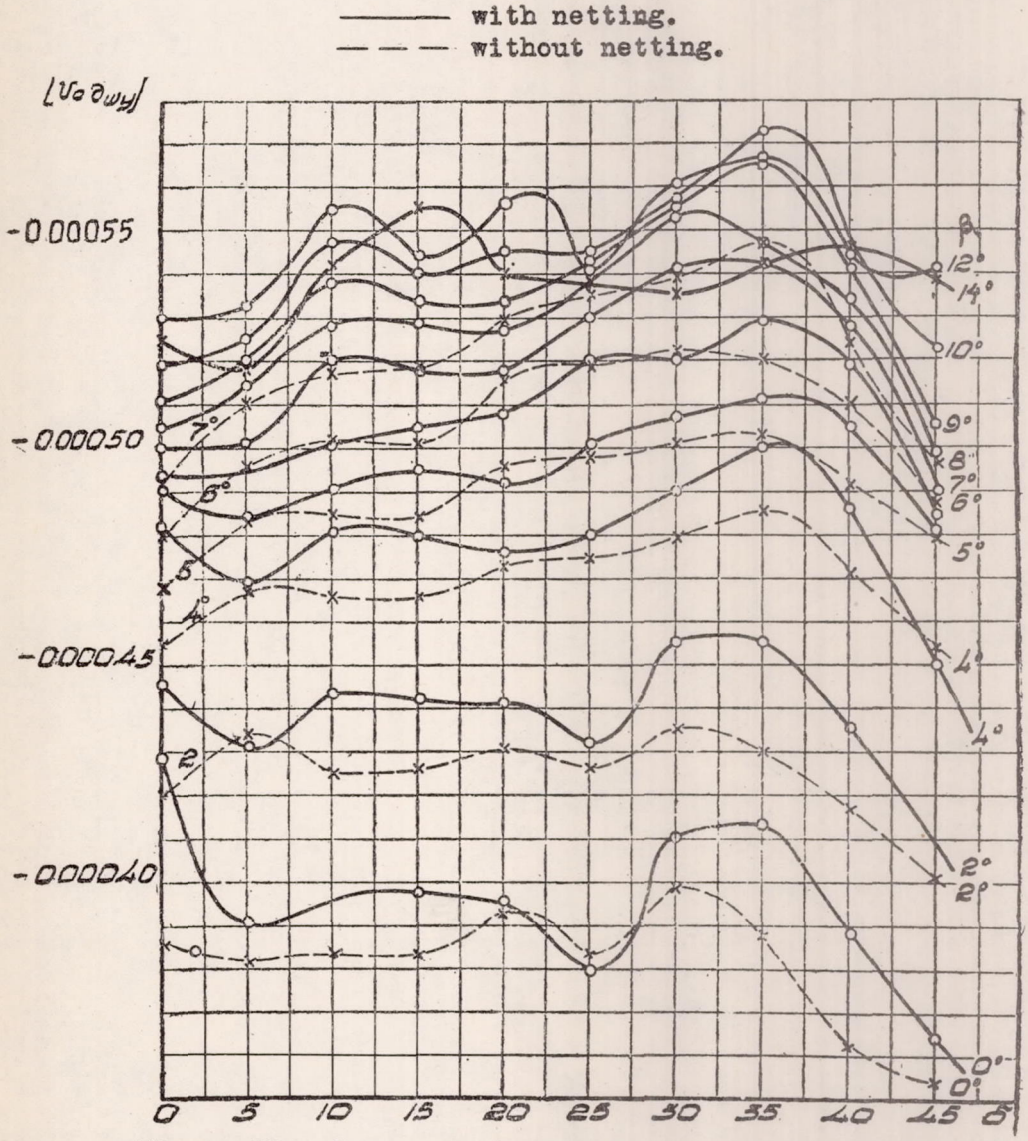


Figure 32.- Curves representing the changes of the moment rotary derivatives of the V-2 model, with reference to the rudder angles of deviation δ, for different β_o (curved model).

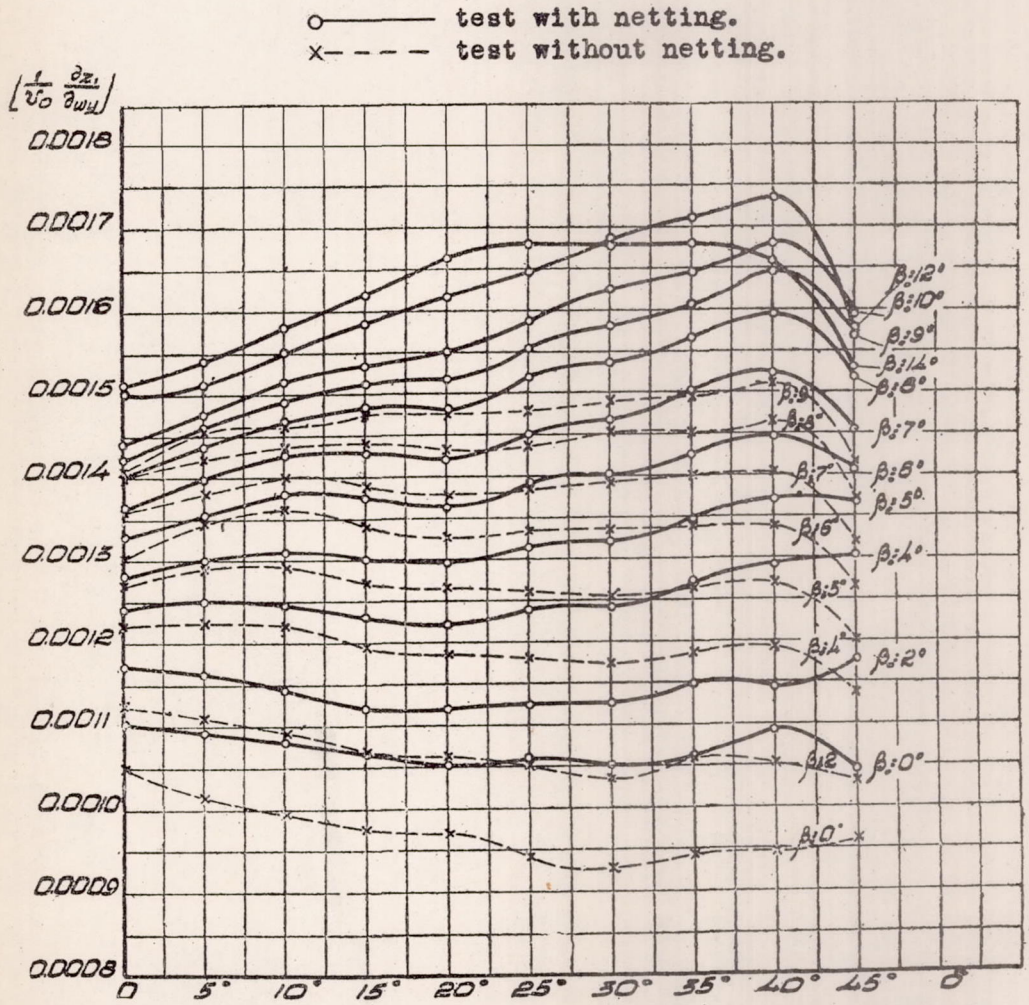


Figure 33.- Change of the rotary derivatives of the lateral aerodynamic forces, with reference to the rudder angle of deviation δ, for different angles of attack β_0 (test with curved V-2 model).

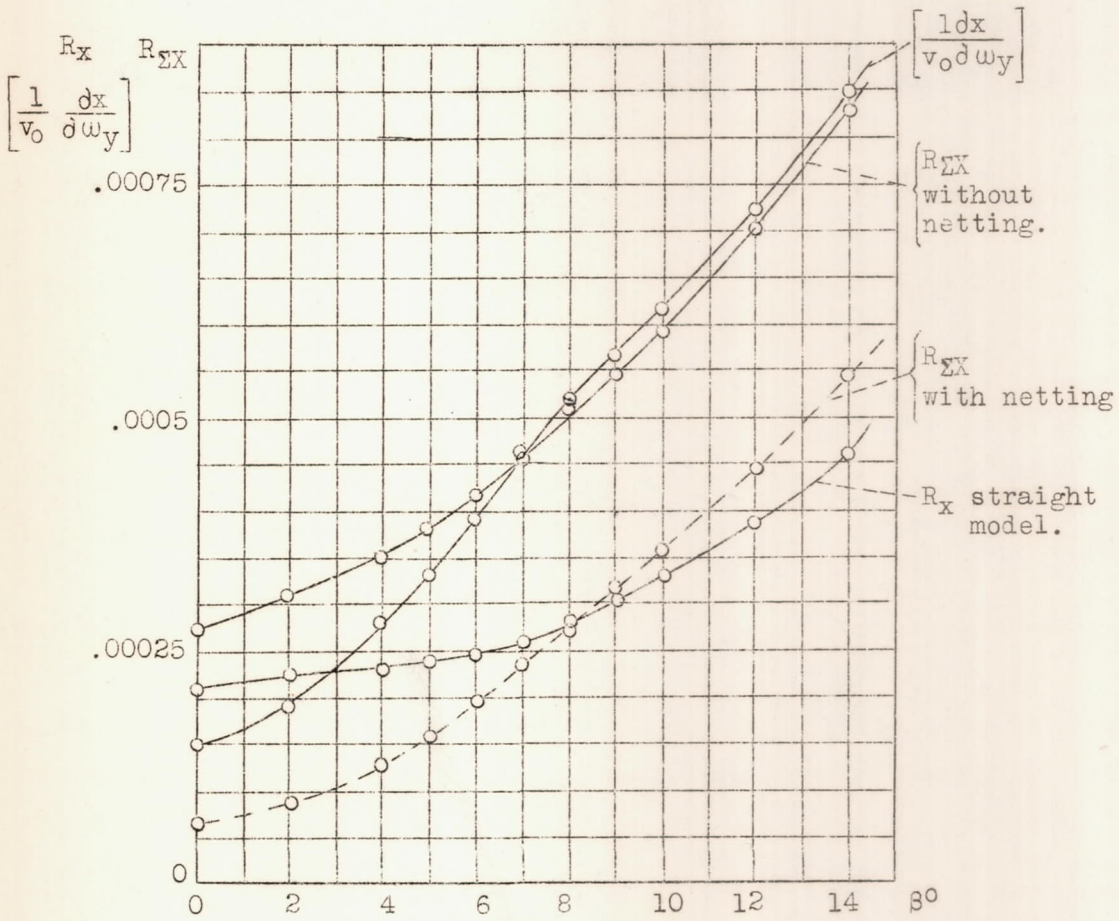


Figure 34.- Value of the coefficients of $R_{\Sigma X}$, R_X and of the rotary derivative of drag as a function of the angle of attack β_o when $\delta=0$ (from the tests of the straight and curved V-2 models).

a, of the full-scale ship(in meters).
b, according to the equation of forces.
c, according to the equation of moments.

$\frac{1}{R_0}$ of the model

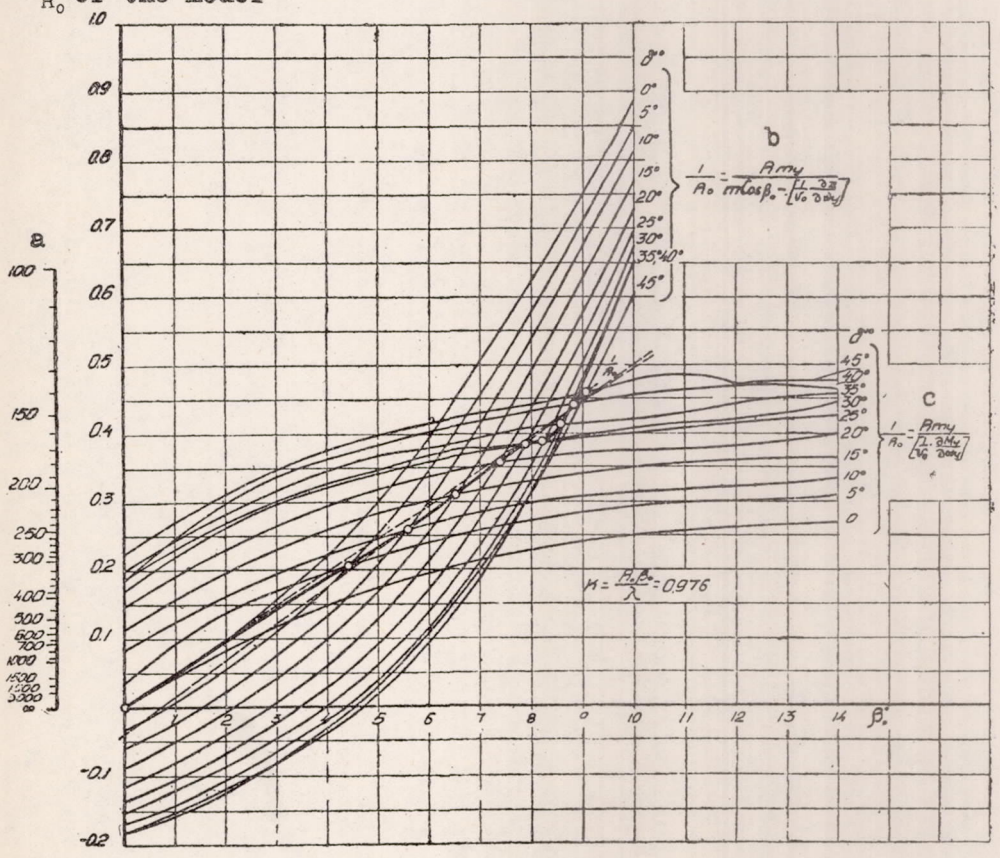


Figure 35.- Relation of $\frac{1}{R_0} = f(\beta_0, \delta)$ for the V-2 model $\left(M = \frac{1}{64.64} \text{ full scale size}\right)$, constructed according to the curved model tests ($R_0 = 2.325$, $\beta_0 = 8^0 51'$) with a velocity gradient.

a, of the full scale ship(in meters).
b, according to the equation of forces.
c, according to the eqoation of moments.
$\frac{1}{R_0}$ of the model.

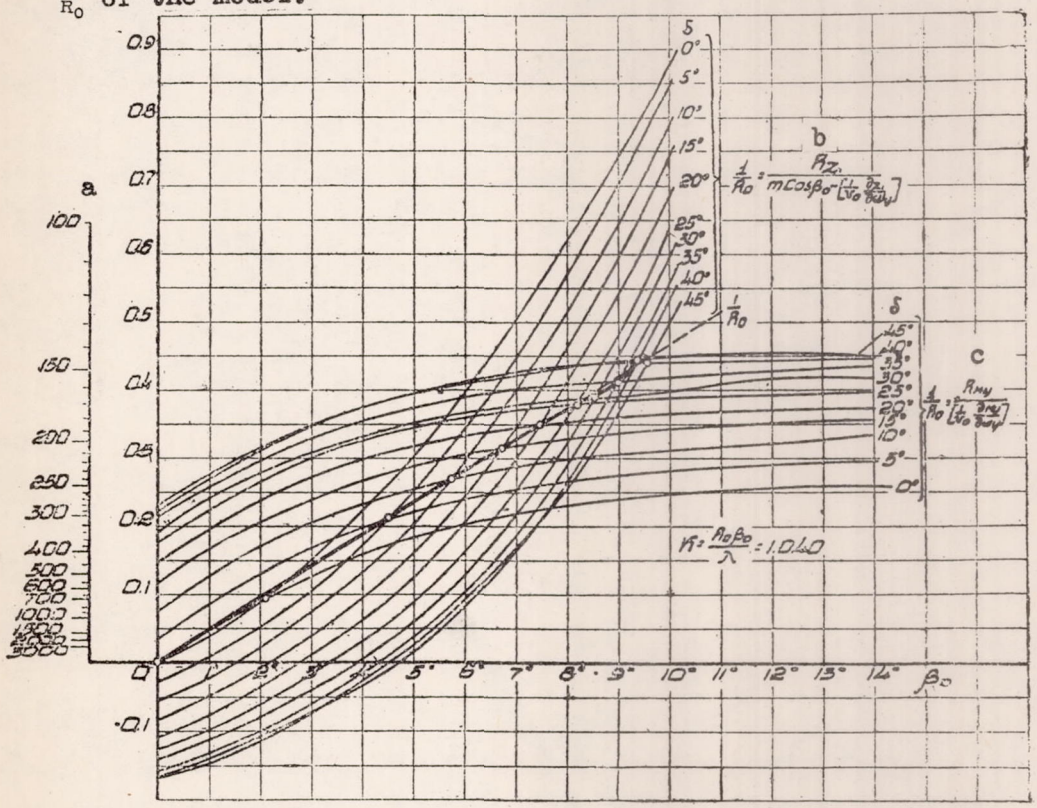


Figure 36.- Relation of $\frac{1}{R_0}$ f (β_0 , δ) for the V-2 model $\left(M = \frac{1}{64.64} \text{ full-scale size}\right)$, constructed according to the curved model tests (R_0=2.325, β_0=8°51') without a velocity gradient.

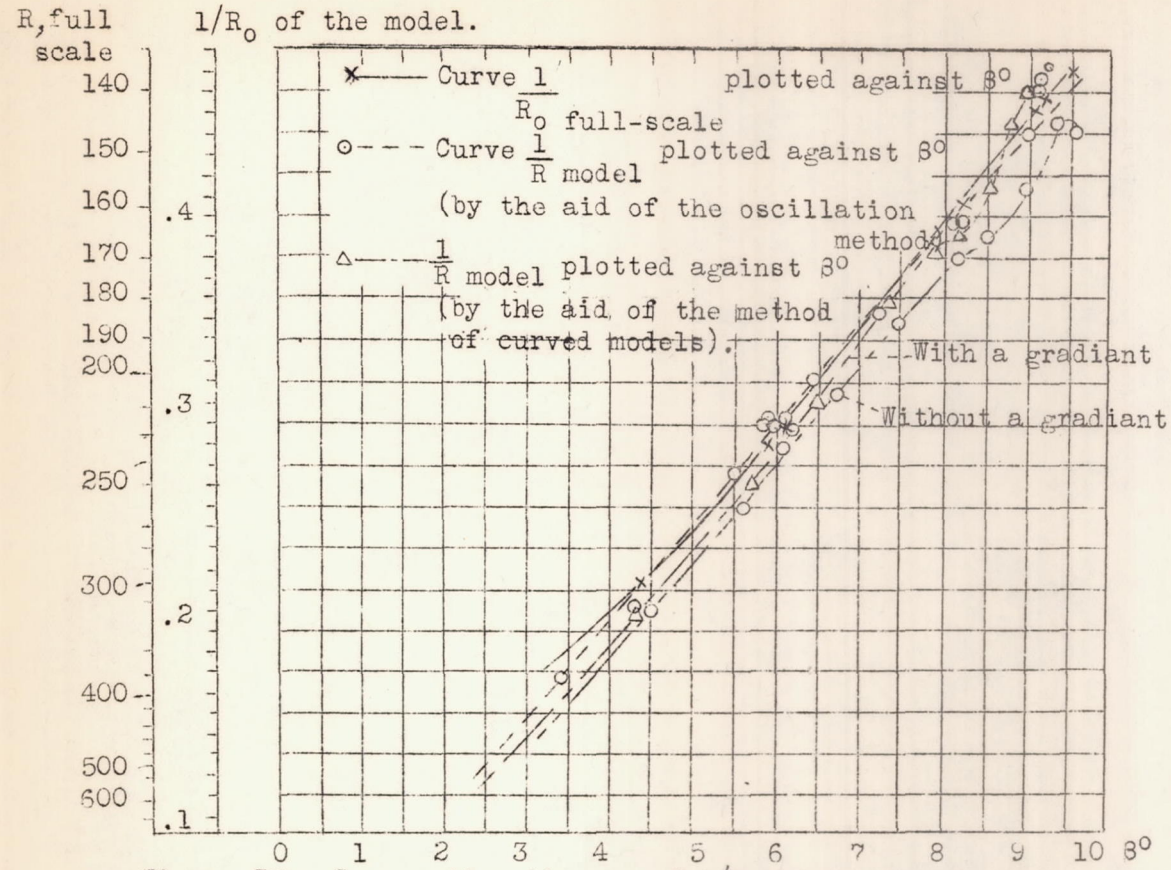


Figure 37.- Comparative diagram of $1/R_o$ plotted against β_o of the free flight test with the V-2 dirigible and the test with the model in the tunnel.

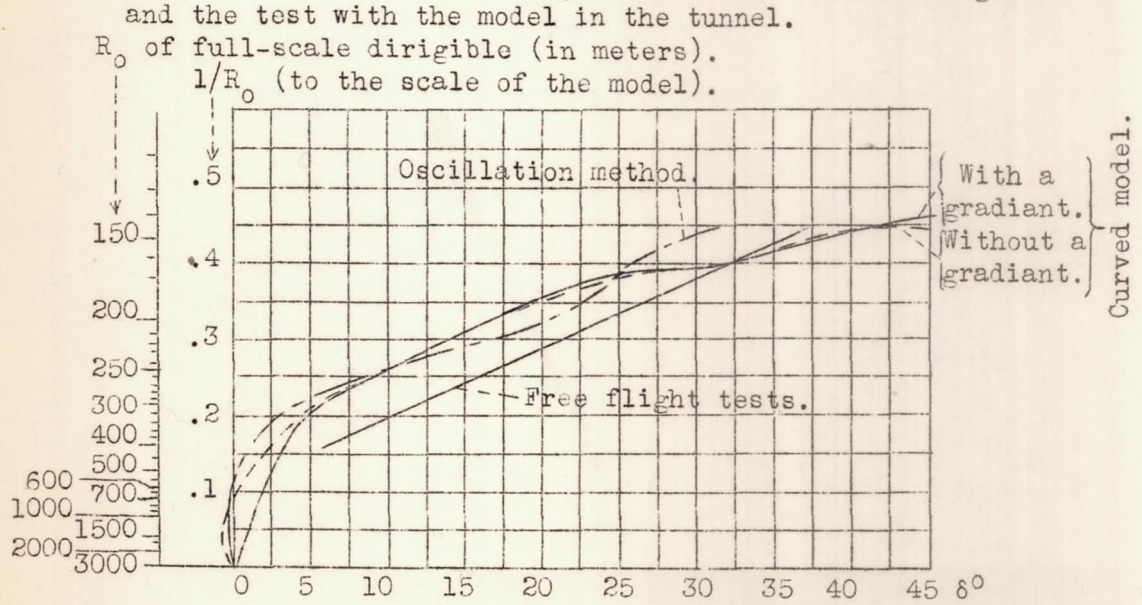


Figure 38.- Value of $1/R_o$ as a function of the rudder angle of deviation (V-2 model and full-scale ship).

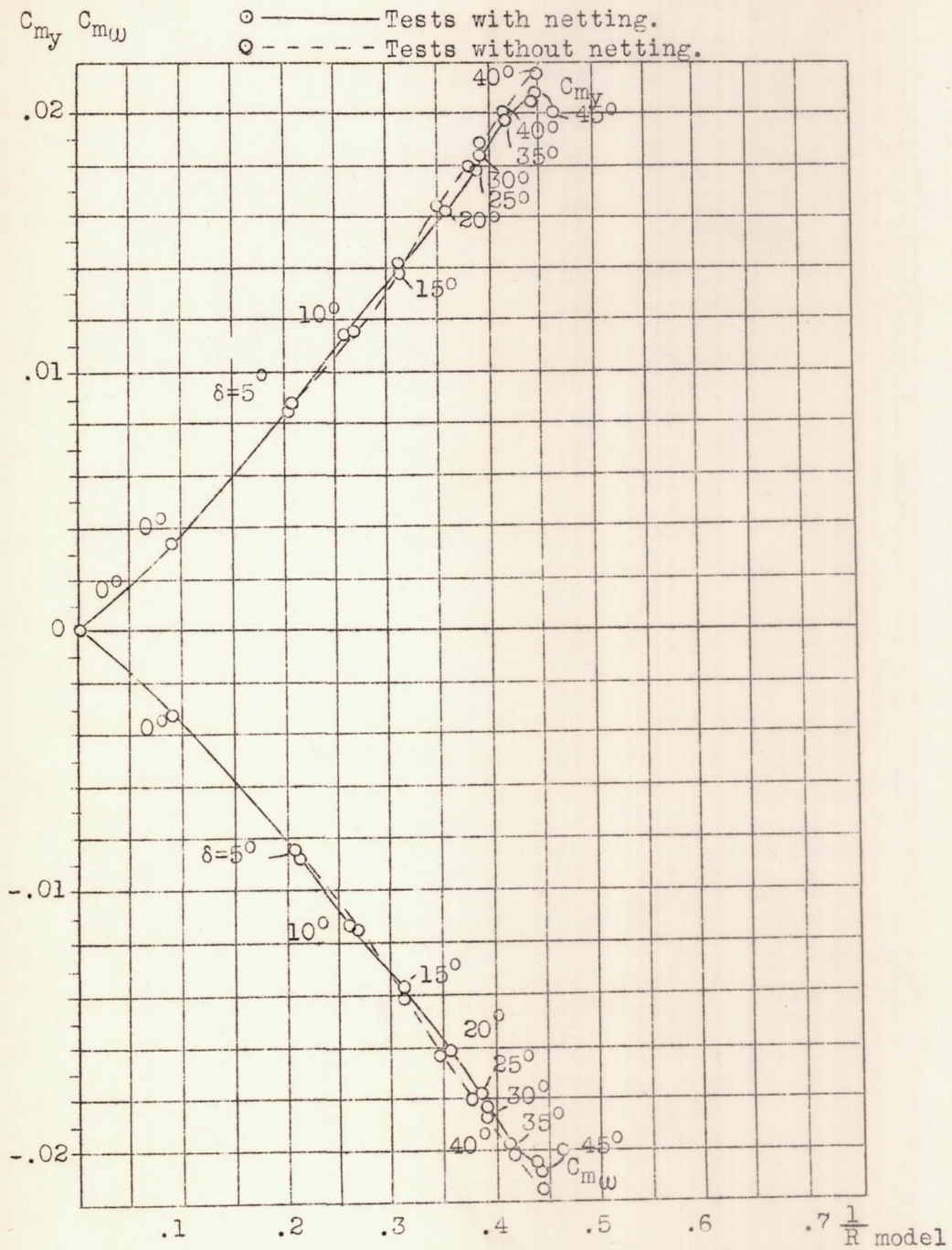


Figure 39.- Value of the non-dimensional coefficients of the linear, rotary and total moments as a function of $1/R_{o\ \text{model}}$. (during circular flight).

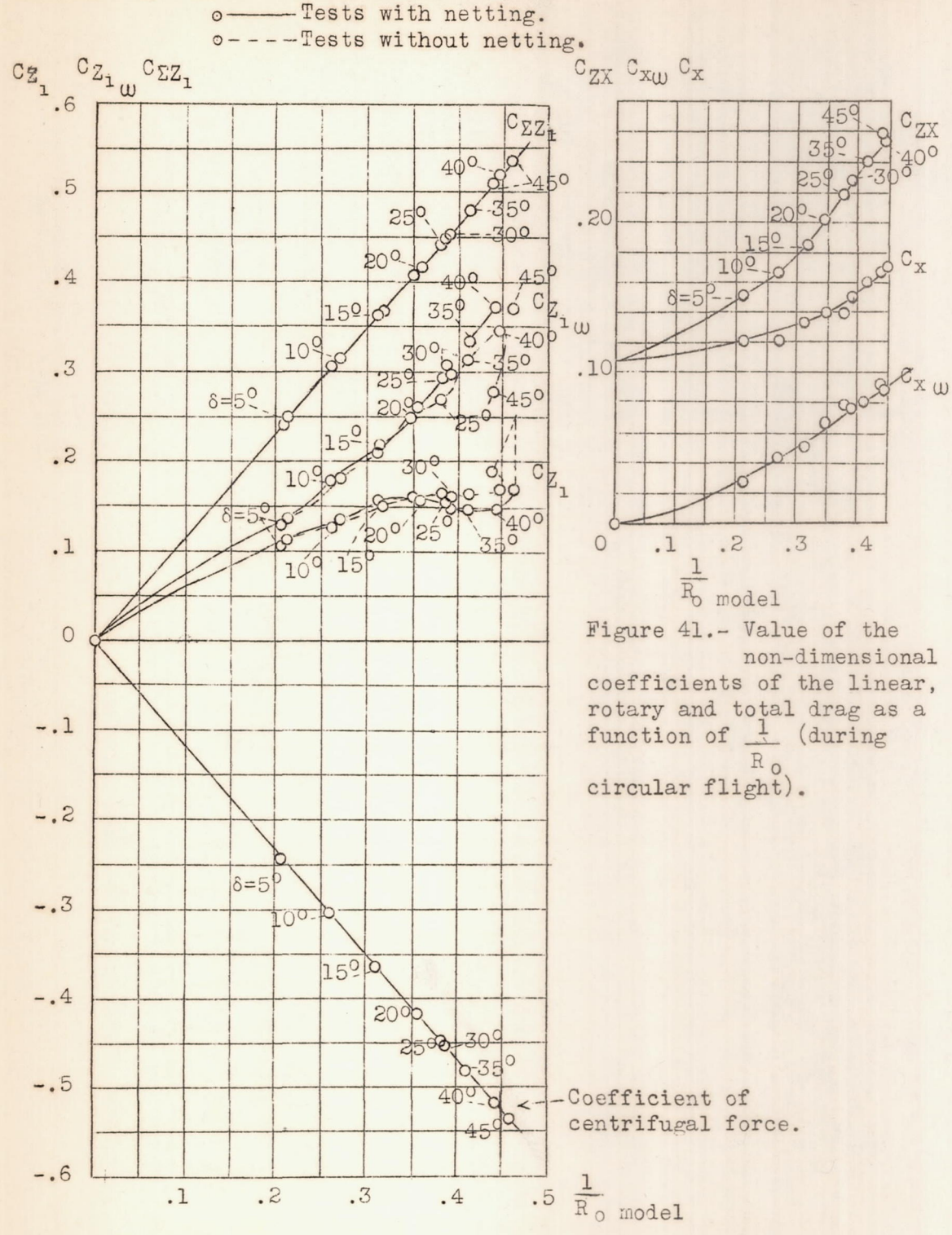


Figure 41.- Value of the non-dimensional coefficients of the linear, rotary and total drag as a function of $\frac{1}{R_o}$ (during circular flight).

Figure 40.- Value of the non-dimensional coefficients of the linear, rotary, total and centrifugal forces as a function of $\frac{1}{R_o \text{ model}}$ (during circular flight).